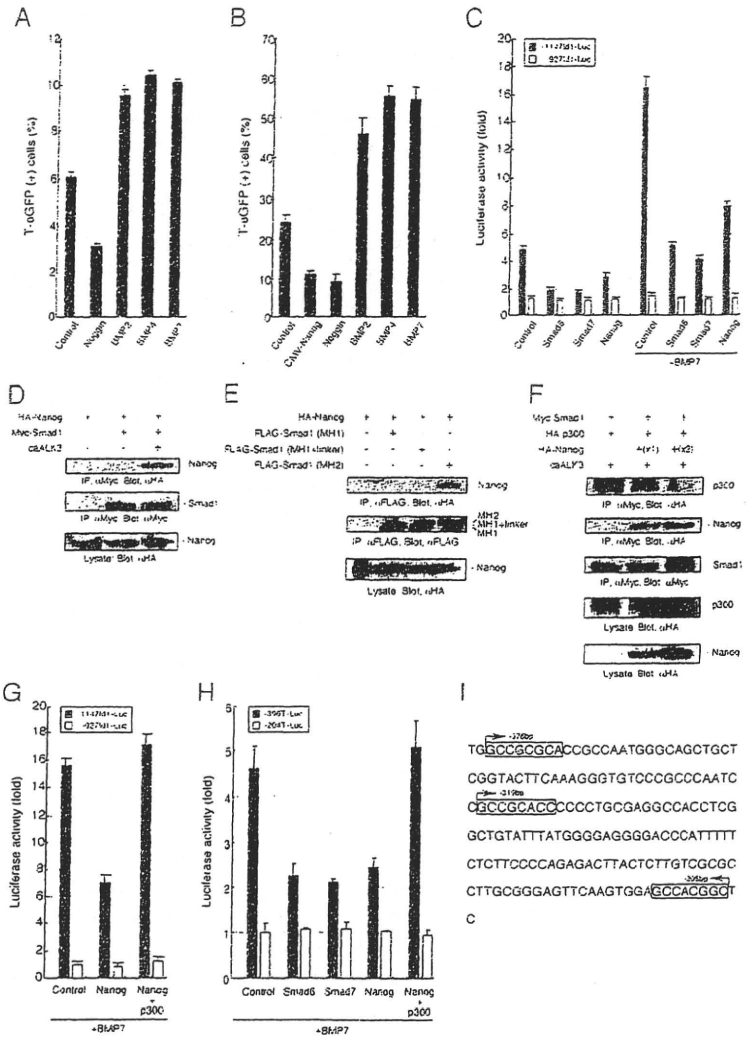

Fig. 6 Nanog interferes with BMP signaling at the level of transcription activity of Smad. (**A**) Flow-cytometric analysis of T(+) cells in *T-eGFP* ES cells cultured for three passages with 400 μ/mL of LIF under conditions of inhibition (noggin) or activation (BMP2, BMP4, and BMP7) of BMP signaling. *Bar* shows mean ± SD (n = 4). (**B**) Flow-cytometric analysis of T(+) cells produced from purified T(+) cells cultured with 400 μ/mL of LIF under conditions of inhibition or activation of BMP signaling. Inhibition of endogenous BMP signaling by noggin decreased the percentage of T(+) cells at a similar level of Nanog overexpression, whereas BMP activation increased the percentage of T(+) cells. *Bar* shows mean ± SD (n = 4). (**C**) A reporter construct of −1147Id1-Luc containing the Smad-binding sites, but not −927Id1-Luc, was activated in a BMP-dependent manner in ES cells cultured with 400 μ/mL of LIF. Nanog and inhibitory Smads (Smad6 and Smad7) down-regulated −1147Id1-Luc activity in a similar manner. Bars show mean ± SD (n = 4). (**D–F**) Co-immunoprecipitation assays of the physical interaction between Nanog and BMP-responsive Smad1. Nanog interacted with activated Smad1 (**D**). Nanog interacted with the MH2 domain of Smad1 (**E**). Nanog interfered with the interaction between activated Smad1 and p300 by competitively binding to Smad1 in a dose-dependent manner (**F**). The relative p300:Nanog ratio was 1:1 or 1:2. (**G**) Overexpression of p300 rescued the down-regulation of −1147Id1-Luc activity induced by *Nanog*. Bars show mean ± SD (n = 4). (**H**) The −396T-Luc reporter construct, but not −204T-Luc, was activated in a BMP-dependent manner in ES cells cultured with 400 u/ml of LIF. Nanog and inhibitory Smads (Smad6 and Smad7) down-regulated −396T-Luc activity in a similar manner. The down-regulation of −396T-Luc activity induced by Nanog was rescued by overexpression of p300. Bars show mean ± SD (n = 4). (**I**) Sequence of the 5′-upstream regulatory region of the mouse *T* gene. Three putative BMP-responsive Smad-binding sites are indicated with boxes. Please, add the following text: Panels A-C and G-I are reproduced with permission of The National Academy of Sciences of the United States of America [49]

to ES cells, whereas the remaining ~25% maintained EM progenitor identity (Fig. 6B, see also Figs. 3E, 3I, 4C). When the cultures were supplemented with BMPs, the maintenance of EM progenitors increased by ~2-fold, whereas it was decreased by half upon incubation with noggin (Fig. 6B). Interestingly, overexpression of *Nanog* in EM progenitors resulted in a decrease in their maintenance similar to that induced by noggin (Fig. 6B). These results indicate that

the generation and maintenance of EM progenitors depends, at least in part, on the differentiation promoting activity of BMPs and suggest that Nanog's ability to reduce the numbers of EM progenitors may depend on the blockade of BMP signaling.

Signaling by BMPs is intracellularly transduced by receptor-regulated Smads (Smad1, 5, and 8) and the co-mediator Smad4 and is antagonized by inhibitory Smads (Smad6 and 7) [34]. To characterize the mechanism by which Nanog blocks BMP signaling, we first analyzed the effects of *Nanog* overexpression in the BMP-induced transcriptional activation of *Id1*. *Id1* is a well-characterized transcriptional target of BMP signaling [35], for which the Smad-binding elements have been mapped to a specific region in the *Id1* promoter [36]. We used luciferase reporter constructs containing (−1147Id1-Luc) or lacking (−927Id1-Luc) the Smad-binding sites [36] and analyzed their activity in ES cells. Transient transfection of these reporters in ES cells resulted in a ~4.5-fold activation of the −1147Id1-Luc reporter when compared to −927Id1-Luc (Fig. 6C), indicating the existence of a significant level of endogenous BMP signaling associated with our culture conditions (see Discussion below). Addition of BMP to the culture medium resulted in a strong up-regulation of the −1147Id1-Luc reporter compared to −927Id1-Luc (Fig. 6C). That the activation of the −1147Id1-Luc reporter was due to BMP signaling was further confirmed by the fact that co-transfection of ES cells with cDNAs encoding inhibitory Smads drastically reduced the transcriptional activity of the reporter induced by endogenous or exogenous BMPs (Fig. 6C). Interestingly, *Nanog* overexpression in ES cells closely mimicked the effect of inhibitory Smads (Fig. 6C), suggesting that Nanog may block BMP signaling by interfering with the formation of activated Smad complexes.

Inhibitory Smads negatively regulate BMP signaling by binding to activated receptor-regulated Smads, hence limiting their availability to form transcriptionally active complexes with Smad4 and/or other nuclear cofactors [34]. To address whether Nanog blocked BMP signaling by a similar mechanism, we first analyzed its ability to interact with the receptor-regulated Smad1 inside the cell. Co-immunoprecipitation assays in NIH3T3 cells revealed that Nanong was indeed able to bind Smad1 only when the latter was activated by co-transfection of a constitutively active ALK3 (caALK3, Fig. 6D). Next, we mapped the interaction domain of Smad1 with Nanog. The different Smads contain two conserved domains, the N-terminal Mad homology (MH) 1 and the C-terminal MH2 domain, separated by a poorly conserved linker. The interaction of receptor-regulated Smads with Smad4 and other transcription factors and cofactors, as well as with inhibitory Smads, occurs through the MH2 domain [34]. In cells co-transfected with Nanog and expression constructs encoding the individual MH1, MH1+linker, or MH2 domains of Smad1, interaction with Nanog was found exclusively with the MH2 domain (Fig. 6E). These results are consistent with a negative role of Nanog on BMP signaling by interfering with the interaction of receptor activated Smads with Smad4 and/or additional nuclear factors.

The paralogous transcriptional coactivators CREB-binding protein (CBP) and p300 are nuclear cofactors important for TGFβ signaling, including that of BMPs, that interact with the MH2 domain of receptor-regulated Smads and Smad4 [37–39]. To gain further insights into the mechanism of Nanog-mediated down regulation of BMP signaling, we tested whether Nanog interfered with the recruitment of p300 to the complexes of activated Smads. For this purpose, Myc-tagged Smad1, HA-tagged p300, and caALK3 were expressed in NIH3T3 cells with or without HA-tagged Nanog. Immunoprecipitations of cell lysates were performed with anti-Myc antibodies followed by Western blotting utilizing anti-HA antibodies. In the absence of Nanog, Smad1 efficiently co-immunoprecipitated p300 (Fig. 6F). In the presence of co-expressed Nanog, the amount of p300 bound to Smad1 decreased in a Nanog dose-dependent manner (Fig. 6F). The functional significance of these findings was further verified by the fact that overexpression of p300 completely rescued the down-regulation in the transcriptional activity of the *Id* promoter induced by Nanog (Fig. 6G). These results indicate that Nanog negatively regulates BMP signaling by interfering with the recruitment of the co-activator p300 to the Smad transcriptional complex.

Finally, the finding that the expression of the *Xbra*, the homologue of *T* in *Xenopus*, is regulated by TGFβ signals [40] prompted us to investigate whether *T* could be a transcriptional target of BMP signaling in ES cells, and, if so, whether Nanog could directly block the induction of *T* by BMPs. In a preliminary analysis, we identified a BMP-responsive element in the ~1.2-kb region upstream of the translation initiation site of the mouse *T* promoter (data not shown). We then generated a series of luciferase reporter constructs covering this region. We transfected these constructs into ES cells cultured in medium containing 400 μ/ml of LIF and supplemented with BMP7, and further mapped the BMP-responsive element to a region located between −396 and −204 bp of the mouse *T* gene (Fig. 6H). Under these conditions, the activity of the −396T-Luc reporter was ~5-fold that of −204T-Luc and decreased by half upon co-expression of inhibitory Smads or Nanog (Fig. 6H). Interestingly, the down-regulation of −396T-Luc activity induced by Nanog could be completely rescued by co-expression of p300 (Fig. 6H). The analysis of this region in the mouse *T* promoter detected three motifs with homology to the reported consensus of BMP-responsive Smad-binding sites [41]. These results indicate that *T* is a direct transcriptional target of BMP signaling, and

that Nanog down-regulates *T* expression by inhibiting BMP signaling at the level of the formation of active Smads/p300 complexes.

8 Discussion

Mouse ES cells, consistent with their developmental origin in the embryo epiblast, have the ability to give rise to derivatives of all three primary germ layers. However, unlike cells in the epiblast, in which pluripotency is very transient, mouse ES cells can be maintained in culture indefinitely in a pluripotent state. The mechanism(s) whereby the adaptation to culture conditions releases epiblast cells from the loss of pluripotency remain an outstanding question in the biology of ES cells.

9 The Transient EM Progenitor Population

In this study, we identify a population of EM progenitors normally present in cultures of mouse ES cells. The commitment of EM progenitors to mesoderm fates is evident upon LIF withdrawal, which results in differentiation restricted to mesoderm lineages and by their failure to contribute to embryogenesis in vivo (Fig. 2A, 2C, 2E). In the presence of LIF, however, EM progenitors are phenotypically indistinguishable from ES cells, as both populations co-exist in colonies of undifferentiated morphology and both maintain pluripotency over extended periods of time in culture (Fig. 1C). Moreover, EM progenitors maintain the expression of pluripotency-associated markers such as *Oct4*, *Nanog*, and *Rex1* and have high levels of alkaline phosphatase activity (Figs. 1B, 3A, and data not shown). Indeed, in the presence of LIF, EM progenitors and ES cells interchange their identities at a rate that depends, precisely, on the amount of LIF.

In this sense, the regeneration of a pluripotent ES cell phenotype from EM progenitors is reminiscent of the reversion to ES cells of early primitive ectoderm-like (EPL) cells [42]. EPL cells are generated in vitro by culturing ES cells in medium conditioned by HepG2 cells with or without LIF [42]. Similar to the population of EM progenitors characterized in this study, EPL cells express markers of pluripotency at levels comparable to ES cells, do not contribute to embryonic lineages upon injection into mouse blastocysts, can be reverted to an ES cell phenotype in the presence of LIF upon withdrawal of HepG2-conditioned medium [42], and differentiate in vitro preferentially (though not exclusively) into mesoderm-derived lineages [43]. EPL cells can be differentiated from ES cells based on their characteristic expression profile, which includes high levels of *Fgf5* expression and down-regulation of *Rex1* and *Gbx2* expression [42]. In contrast, EM progenitors display expression levels of *Rex1* and *Gbx2* comparable to ES cells and do not express *Fgf5* (Fig. 3A). Thus, despite some similarities, EM progenitor cells are distinct from EPL cells and are more closely related to pluripotent ES cells, at least based on their respective transcriptional profiles. In addition, two important characteristics of the EM progenitor population make its analysis especially relevant for our understanding of ES cell pluripotency: (i) EM progenitors are generated from ES cells under standard culture conditions, not by addition of ill-characterized conditioned media, and (ii) in the same culture conditions, EM progenitors undergo a dedifferentiation process that gives rise to pluripotent ES cells.

10 Differentiation-Promoting Activity of BMPs

The results from our analyses indicate that the generation of EM progenitors from ES cells depends on the direct mesoderm-inducing ability of BMP stimulation (Fig. 6). This finding is consistent with the reported roles of BMP signaling during embryo development [27, 28], and with previous studies of ES cell differentiation in vitro [29–31]. However, the mesoderm-differentiating activity of BMPs seems to be at odds with their role in maintaining the self-renewal of pluripotent ES cells [7]. Indeed, BMP signaling appears to have contrasting effects in the maintenance of ES cell pluripotency. On the one hand, BMPs are necessary to prevent ES cell differentiation toward neural fates [7, 30, 44]. On the other hand, signaling by BMPs results in loss of ES cell pluripotency by promoting their differentiation toward non-neural fates such as mesoderm-derived lineages [29, 31] (and this study). These opposing effects of BMPs can be partially explained by differences in the experimental conditions used in those studies: Thus, in the absence of LIF, low concentrations of BMPs (~0.25–10 ng/mL) promote mesoderm differentiation [29–31] at the expense of neural fates [30]. In the presence of LIF, however, similar low concentrations of BMPs prevent neural differentiation of ES cells [7, 44] and maintain their pluripotency with no signs of mesoderm differentiation [7]. Consistent with this notion, we did not detect increased generation of EM progenitors with BMP concentrations below 100 ng/mL in the presence of LIF (data not shown). Thus, LIF appears to render ES cells refractory to the mesoderm-inducing activity of BMPs. Our studies demonstrate that this resistance is, at least in part, dependent on the negative feedback mechanism mediated by Nanog.

11 A Negative Feedback that Blocks Mesoderm Differentiation

While investigating the role of LIF in the maintenance of mouse ES cell pluripotency, Rathjen and colleagues [45] found that the expression of *Lif* itself is up-regulated in the

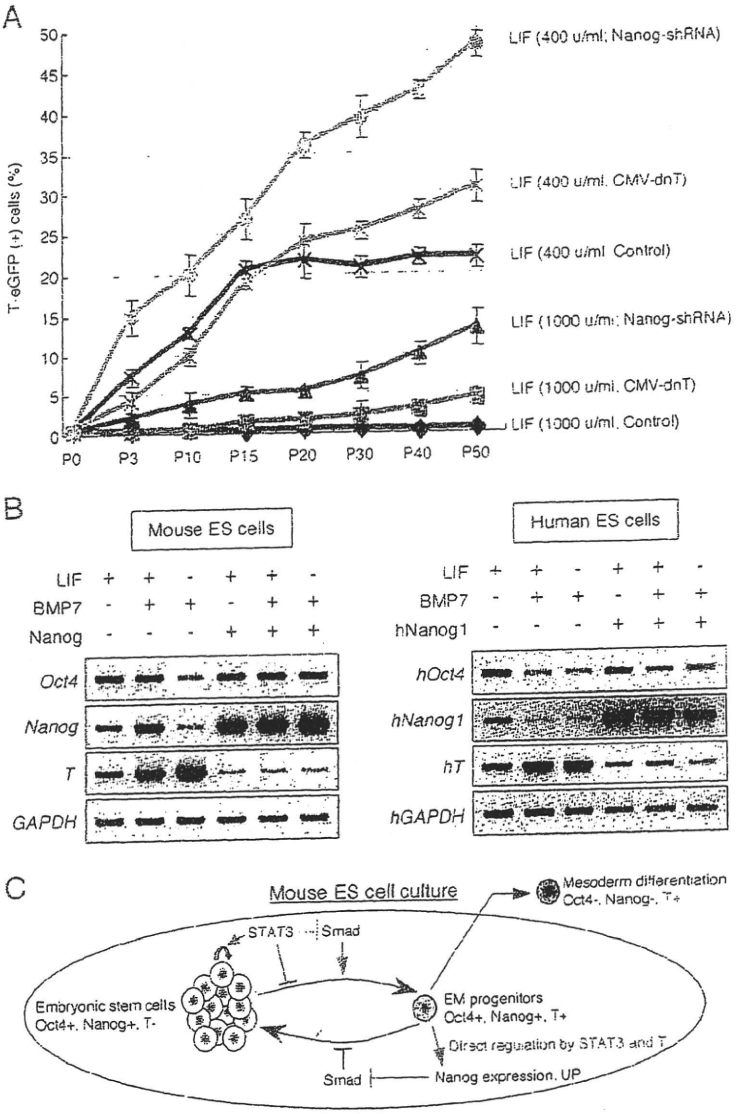

Fig. 7 Nanog-mediated dedifferentiation of EM progenitors is required for maintaining mouse ES cells. (A) Flow-cytometric analysis of T(+) cells in *T-eGFP* ES cells (1000 or 400 u/ml of LIF), after down-regulation of T or Nanog activities with *dnT* or *Nanog-shRNA*. (B) Comparison of expression profiles of mouse and human ES cells. Mouse and human ES cells were transfected with mouse *Nanog* and *hNanog1*, respectively, or a control vector, then treated with LIF and/or BMP7. In human ES cells, *hNanog1* was down-regulated in response to BMP7 stimulation, whereas *T* expression increased. In contrast, in mouse ES cells, these genes were up-regulated by LIF and BMP7. (C) Schematic representation of the mechanism for the maintenance of pluripotent mouse ES cells. EM progenitors are generated in ES cell cultures depending on the balance between the level of LIF/STAT3 and BMP/Smad activation. *Nanog* expression increases in EM progenitors by the combinatorial action of T and activated STAT3. As a result, Nanog inhibits the differentiation signal of BMP by interfering with the formation of activated Smad/p300 complexes, and promotes the dedifferentiation of EM progenitors into pluripotent ES cells. See main text for details

early phases of ES cell differentiation. This mechanism provides a negative feedback that may limit the progression of ES cell differentiation and contribute to the self-renewal of pluripotent ES cells [45]. The transition of EM progenitors to ES cells does not appear to depend on such a mechanism, since *Lif* expression is not noticeably up-regulated in EM progenitors (Fig. 3A). In contrast, EM progenitors do up-regulate the expression of *Nanog* (Fig. 3A). Our results also show that, in the presence of LIF, *Nanog* overexpression is sufficient to accelerate the transition of EM progenitors to ES cells (Fig. 3F, 3H, 3J). More importantly, down-regulation of Nanog function results in impaired dedifferentiation of EM progenitors to ES cells (Fig. 3G, 3H, and 3K). Thus, we identify Nanog as a critical component of

a negative feedback mechanism that blocks the progression of ES cell differentiation toward mesoderm fates (Fig. 7C). In this mechanism, mesoderm differentiation of ES cells is initiated by BMP signaling. Possible sources of BMP activity in our culture conditions include fetal calf serum [29], fibroblast feeder layer, and/or ES cells themselves [7]. Consistent with this, we detect a significant activation of the -1147Id1-Luc reporter even in the absence of exogenous BMP supplements (Fig. 6C). ES cells that initiate mesoderm differentiation express the early mesoderm marker *T*. In the presence of LIF, activated STAT3 cooperates with T to directly up-regulate the expression of *Nanog* (Fig. 5), which, in turn, provides a negative feedback that down-regulates *T* expression and eventually leads to the regeneration of ES cells from EM progenitors. In the absence of LIF/STAT3 signaling, T is not sufficient to up-regulate the expression of *Nanog*, and mesoderm differentiation proceeds. The relevance of this negative feedback mechanism for maintaining the pluripotency of ES cells is evident in long-term cultures. Thus, the size of the EM population cannot be maintained in ES cells in which either Nanog or T function is experimentally down-regulated (Fig. 7A). In such conditions, the cultures progressively accumulate EM progenitors and eventually lose pluripotency (not shown).

The existence of such a negative feedback mechanism in mouse ES cells contributes to explaining previous observations on the function of Nanog. For instance, the fact that overexpression of *Nanog* bypasses the need for LIF/STAT3 signaling [10] and BMP stimulation [7] to maintain self-renewal of pluripotent ES cells is easily understood in light of this mechanism. Since the final outcome of BMP activity is the up- regulation of *Nanog* expression, which is mediated by LIF/STAT3 signaling, the experimental up-regulation of Nanog would obviate the need for both BMP and LIF. It is clear, however, that the functions of LIF and Nanog in the maintenance of ES cell pluripotency are not restricted to participating in the negative feedback mechanism characterized in this study. Thus, the complete lack of Nanog function promotes differentiation of ES cells to endoderm lineages [9], indicating the existence of additional roles of Nanog other than that of preventing mesoderm differentiation. Indeed, the up-regulation of *Nanog* expression by T and STAT3 only takes place in EM progenitors, whereas the constitutive expression of *Nanog* in ES cells is regulated by more proximal regions of the *Nanog* promoter (Fig. 5E).

The requirement of LIF/STAT3 signaling for the maintenance of mouse ES cells has been related to the ability of pre-implantation mouse embryos to arrest development when implantation is prevented (a phenomenon known as dispause) [46]. In keeping with this idea, it appears reasonable that cells in the inner cell mass of mouse blastocysts evolve specific mechanisms to prevent unwanted cell differentiation during dispause. The mechanism described in this study could very well serve this purpose. In contrast, ES cells derived from human embryos, in which dispause does not occur, do not depend on LIF/STAT3 signaling to maintain pluripotency [47]. Interestingly, the Nanog-mediated negative feedback mechanism characterized in this study does not appear to be operative in human ES cells. First, the overall conservation of the mouse *Nanog* EM-enhancer in the human *Nanog* gene is very poor, and no T-binding site is present (not shown). Second, unlike mouse ES cells, human ES cells do not up-regulate *Nanog* expression in response to LIF and BMP stimulation, even though *T* expression is induced under these conditions (Fig. 7B). The absence of a functional negative feedback mechanism mediated by T, LIF/STAT3, and Nanog in human ES cells provides additional mechanistic insights into the reasons why LIF is dispensable for the self-renewal of human ES cells.

Taken together, our results uncover a mechanism underlying mouse ES cell pluripotency, by which committed mesoderm progenitors undergo an active process of dedifferentiation mediated by the combined action of the extrinsic cytokine LIF and the intrinsic pluripotency factor Nanog. These findings contribute to unravel the complex network of molecular interactions required to maintain the self-renewal of ES cells and shed light on the cellular bases of ES cell pluripotency. Furthermore, the possibility of reverting the differentiation status of committed cells offers new ways to approach the generation of pluripotent cells for future therapeutic interventions of regenerative medicine.

Acknowledgments We thank Robert Benezra, Senyon Choe, Neil G. Copeland, Richard Eckner, Douglas Melton, Kohei Miyazono, Gustavo Tiscornia, and Shinya Yamanaka for sharing reagents, Dirk Buscher, Chris Kintner, Isao Oishi, Junichiro Sonoda, and Ayumu Tashiro for helpful suggestions, Harley Pineda, Timothy Chapman, and Henry Juguilon for excellent technical assistance, and May-Fun Schwarz for help in the preparation of this manuscript. AS was partially supported by JSPS Research Fellowships for Young Scientists, Japan; AS, TM, and KN are partially supported by JSPS Postdoctoral Fellowships for Research Abroad, Japan; AR and CRE are partially supported by postdoctoral fellowships from Fundación Inbiomed, Spain. The authors are indebted to the Salk Institute administration for the establishment of a non-NIH core in the Stem Cell Research Center through support of institutional funds, the Lookout Fund, and the G. Harold and Leila Y. Mathers Charitable Foundation. Additional funding for mouse ES cell work in JCIB's laboratory was from the G. Harold and Leila Y. Mathers Charitable Foundation and the NIH.

References

1. Martin GR. Isolation of a pluripotent cell line from early mouse embryos cultured in medium conditioned by teratocarcinoma stem cells. Proc Natl Acad Sci U S A. 1981;78:7634–8.
2. Evans MJ, Kaufman MH. Establishment in culture of pluripotential cells from mouse embryos. Nature. 1981;292:154–6.

3 Smith AG. Embryo-derived stem cells: of mice and men. Annu Rev Cell Dev Biol. 2001;17:435–62.
4 Chambers I, Smith A. Self-renewal of teratocarcinoma and embryonic stem cells. Oncogene. 2004;23:7150–60.
5 Smith AG, Heath JK, Donaldson DD, et al. Inhibition of pluripotential embryonic stem cell differentiation by purified polypeptides. Nature. 1988;336:688–90.
6 Williams RL, Hilton DJ, Pease S, et al. Myeloid leukaemia inhibitory factor maintains the developmental potential of embryonic stem cells. Nature. 1988;336:684–7.
7 Ying QL, Nichols J, Chambers I, et al. BMP induction of Id proteins suppresses differentiation and sustains embryonic stem cell self-renewal in collaboration with STAT3. Cell. 2003;115:281–92.
8 Nichols J, Zevnik B, Anastassiadis K, et al. Formation of pluripotent stem cells in the mammalian embryo depends on the POU transcription factor Oct4. Cell. 1998;95:379–91.
9 Mitsui K, Tokuzawa Y, Itoh H, et al. The homeoprotein Nanog is required for maintenance of pluripotency in mouse epiblast and ES cells. Cell. 2003;113:631–42.
10 Chambers I, Colby D, Robertson M, et al. Functional expression cloning of Nanog, a pluripotency sustaining factor in embryonic stem cells. Cell. 2003;113:643–55.
11 Niwa H, Miyazaki J, Smith AG. Quantitative expression of Oct-3/4 defines differentiation, dedifferentiation or self-renewal of ES cells. Nat Genet. 2000;24:372–6.
12 Shamblott MJ, Axelman J, Wang S, et al. Derivation of pluripotent stem cells from cultured human primordial germ cells. Proc Natl Acad Sci U S A. 1998;95:13726–31.
13 Thomson JA, Itskovitz-Eldor J, Shapiro SS, et al. Embryonic stem cell lines derived from human blastocysts. Science. 1998;282:1145–7.
14 Rao M. Conserved and divergent paths that regulate self-renewal in mouse and human embryonic stem cells. Dev Biol. 2004;275:269–86.
15 Herrmann BG, Labeit S, Poustka A, et al. Cloning of the T gene required in mesoderm formation in the mouse. Nature. 1990;343:617–22.
16 Wilkinson DG, Bhatt S, Herrmann BG. Expression pattern of the mouse T gene and its role in mesoderm formation. Nature. 1990;343:657–9.
17 Ramalho-Santos M, Yoon S, Matsuzaki Y, et al. "Stemness": transcriptional profiling of embryonic and adult stem cells. Science. 2002;298:597–600.
18 Raz R, Lee CK, Cannizzaro LA, et al. Essential role of STAT3 for embryonic stem cell pluripotency. Proc Natl Acad Sci U S A. 1999;96:2846–51.
19 Gossen M, Freundlieb S, Bender G, et al. Transcriptional activation by tetracyclines in mammalian cells. Science. 1995;268:1766–9.
20 Hoffmann A, Czichos S, Kaps C, et al. The T-box transcription factor Brachyury mediates cartilage development in mesenchymal stem cell line C3H10T1/2. J Cell Sci. 2002;115:769–81.
21 Kispert A, Herrmann BG. The Brachyury gene encodes a novel DNA binding protein. EMBO J. 1993;12:3211–20.
22 Hiroi Y, Kudoh S, Monzen K, et al. Tbx5 associates with Nkx2-5 and synergistically promotes cardiomyocyte differentiation. Nat Genet. 2001;28:276–80.
23 Stennard FA, Costa MW, Elliott DA, et al. Cardiac T-box factor Tbx20 directly interacts with Nkx2-5, GATA4, and GATA5 in regulation of gene expression in the developing heart. Dev Biol. 2003;262:206–24.
24 Garg V, Kathiriya IS, Barnes R, et al. GATA4 mutations cause human congenital heart defects and reveal an interaction with TBX5. Nature. 2003;424:443–7.
25 Zhu M, John S, Berg M, et al. Functional association of Nmi with Stat5 and Stat1 in IL-2- and IFNgamma-mediated signaling. Cell. 1999;96:121–30.
26 Collum RG, Brutsaert S, Lee G, et al. A Stat3-interacting protein (StIP1) regulates cytokine signal transduction. Proc Natl Acad Sci U S A. 2000;97:10129–34.
27 Dale L, Howes G, Price BM, et al. Bone morphogenetic protein 4: a ventralizing factor in early Xenopus development. Development. 1992;115:573–85.
28 Jones CM, Lyons KM, Lapan PM, et al. DVR-4 (bone morphogenetic protein-4) as a posterior-ventralizing factor in Xenopus mesoderm induction. Development. 1992;115:639–55.
29 Johansson BM, Wiles MV. Evidence for involvement of activin A and bone morphogenetic protein 4 in mammalian mesoderm and hematopoietic development. Mol Cell Biol. 1995;15:141–51.
30 Finley MF, Devata S, Huettner JE. BMP-4 inhibits neural differentiation of murine embryonic stem cells. J Neurobiol. 1999;40:271–87.
31 Czyz J, Wobus A. Embryonic stem cell differentiation: the role of extracellular factors. Differentiation. 2001;68:167–74.
32 Holley SA, Neul JL, Attisano L, et al. The Xenopus dorsalizing factor noggin ventralizes Drosophila embryos by preventing DPP from activating its receptor. Cell. 1996;86:607–17.
33 Zimmerman LB, De Jesus-Escobar JM, Harland RM. The Spemann organizer signal noggin binds and inactivates bone morphogenetic protein 4. Cell. 1996;86:599–606.
34 Shi Y, Massague J. Mechanisms of TGF-beta signaling from cell membrane to the nucleus. Cell. 2003;113:685–700.
35 Hollnagel A, Oehlmann V, Heymer J, et al. Id genes are direct targets of bone morphogenetic protein induction in embryonic stem cells. J Biol Chem. 1999;274:19838–45.
36 Nakashima K, Takizawa T, Ochiai W, et al. BMP2-mediated alteration in the developmental pathway of fetal mouse brain cells from neurogenesis to astrocytogenesis. Proc Natl Acad Sci U S A. 2001;98:5868–73.
37 Feng XH, Zhang Y, Wu RY, et al. The tumor suppressor Smad4/DPC4 and transcriptional adaptor CBP/p300 are coactivators for smad3 in TGF-beta-induced transcriptional activation. Genes Dev. 1998;12:2153–63.
38 Janknecht R, Wells NJ, Hunter T. TGF-beta-stimulated cooperation of smad proteins with the coactivators CBP/p300. Genes Dev. 1998;12:2114–9.
39 Pearson KL, Hunter T, Janknecht R. Activation of Smad1-mediated transcription by p300/CBP. Biochim Biophys Acta. 1999;1489:354–64.
40 Latinkic BV, Umbhauer M, Neal KA, et al. The Xenopus Brachyury promoter is activated by FGF and low concentrations of activin and suppressed by high concentrations of activin and by paired-type homeodomain proteins. Genes Dev. 1997;11:3265–76.
41 Kim I, Johnson K, Chen HJ, et al. Drosophila Mad binds to DNA and directly mediates activation of vestigial by Decapentaplegic. Nature. 1997;388:304–8.
42 Rathjen J, Lake JA, Bettess MD, et al. Formation of a primitive ectoderm like cell population, EPL cells, from ES cells in response to biologically derived factors. J Cell Sci. 1999;112(Pt 5):601–12.
43 Lake J, Rathjen J, Remiszewski J, et al. Reversible programming of pluripotent cell differentiation. J Cell Sci. 2000;113(Pt 3):555–66.
44 Tropepe V, Hitoshi S, Sirard C, et al. Direct neural fate specification from embryonic stem cells: a primitive mammalian neural stem cell stage acquired through a default mechanism. Neuron. 2001;30:65–78.

45 Rathjen PD, Nichols J, Toth S, et al. Developmentally programmed induction of differentiation inhibiting activity and the control of stem cell populations. Genes Dev. 1990;4:2308-18.
46. Nichols J, Chambers I, Taga T, et al. Physiological rationale for responsiveness of mouse embryonic stem cells to gp130 cytokines. Development. 2001;128:2333-9.
47. Daheron L, Opitz SL, Zaehres H, et al. LIF/STAT3 signaling fails to maintain self-renewal of human embryonic stem cells. Stem Cells. 2004;22:770-8.
48 Suzuki A, Raya A, Kawakami Y, et al. Maintenance of embryonic stem cell pluripotency by Nanog-mediated reversal of mesoderm specification. Nat Clin Pract Cardiovasc Med. 2006;3 Suppl 1:S114-22.
49 Suzuki A, Raya A, Kawakami Y, et al. Nanog binds to Smad1 and blocks bone morphogenetic protein-induced differentiation of embryonic stem cells. Proc Natl Acad Sci U S A. 2006;103:10294-9.

Behavioural Brain Research 213 (2010) 126–129

Contents lists available at ScienceDirect

Behavioural Brain Research

journal homepage: www.elsevier.com/locate/bbr

Short communication

Strain differences of selective attention in mice: Effect of Kamin blocking on classical fear conditioning

Kazuyuki Yamada *

Support Unit for Animal Experiments, Research Resources Center, Brain Science Institute (BSI), The Institute of Physical and Chemical Research (RIKEN), 2-1 Hirosawa, Wako-city, Saitama 351-0198, Japan

ARTICLE INFO

Article history:
Received 6 January 2010
Received in revised form 20 April 2010
Accepted 23 April 2010
Available online 29 April 2010

Keywords:
Kamin blocking effect
Classical fear conditioning
Contextual conditioning
Selective attention
Strain difference
Schizophrenia

ABSTRACT

Selective attention was assessed in mice using a classical fear conditioning procedure. Mice were trained by three regimens involving contextual and/or cued conditioning (classical fear conditioning). Most notably, C57BL/6J mice exhibited salient contextual blocking, whereas DBA/2J and ICR mice did not. This study provides a new method to assess the selective attention of mice and describes an animal model for certain human mental disorders, such as schizophrenia.

In traditional learning theory, it has been proposed that after an initial conditioned stimulus (CS1) is learned to predict an outcome, a second conditioned stimulus (CS2) presented in combination with CS1 that leads to the same outcome cannot be learned to predict the outcome completely. This phenomenon is called blocking (Kamin blocking effect) [11]. The principle of blocking provides a model for investigating the selective attention process in animals and humans [6,11,12]. Selective attention is one of the principle mechanisms for information processing, especially with respect to how an organism obtains the information it needs (e.g., cocktail party effect) [3]. Disruption of attention leads to the breakdown of normal information processing, and causes some mental disorders such as schizophrenia in humans [1,13]. Some studies have reported schizophrenia patients that exhibited a disrupted blocking effect [2,7,9,10,15,16]. Therefore, blocking protocols provide not only useful tools for screening humans for schizophrenia, but also unique animal models for studying mental disorders.

One of the most basic procedures for studying the blocking effect uses the conditioned emotional response (CER) in rats [11,17,18,22]. In CER experiments, rats are first trained an instrumental behavior such as lever pressing (reinforced by a reward such as a food pellet) or licking (reinforced by a reward such as water). When they have acquired the desired behavior, the rats are trained by classical fear conditioning using a tone or light as a conditioned stimulus (CS) and an electric foot shock as an unconditioned stimulus (US). In the test trial, the rats are again exposed to the instrumental and/or appetitive behavior situation and eventually the CS. During CS presentation, rate of lever pressing or licking is suppressed by the "memory of fear experience". In the classical fear conditioning phase of a blocking study, the first CS (e.g., light) is conditioned to foot shocks, and the second CS (e.g., tone) is conditioned to foot shocks with light. During the subsequent training phase, the rats suppress their lever pressing or licking when a light CS is presented, but do not suppress their behavior when a tone CS is presented.

Although this procedure is simple and the results are reproducible, a long training period is required for instrumental conditioning. Furthermore, this procedure is quite difficult to adapt for mice, which do not press levers, poke holes or lick water as frequently as rats. This presents a serious limitation, because animal models for mental disorders have been shifting from rats to genetically modified mice, such as transgenic (TG) and knockout (KO) mice [5,24,25]. Moreover, as screening of genetically modified mice often relies on high-throughput procedures, more simple procedures for blocking experiments are needed.

Another procedure used to assess attention mechanisms in mice is latent inhibition, in which mice are exposed to a CS without a prior US conditioning trial [14,20]. This method is very simple and is frequently used for phenotyping genetically engineered mice. Although, the "memory" that inhibits the second conditioning in a

* Tel.: +81 48 467 7659; fax: +81 48 467 6287.
E-mail address: kaz-yamada@brain.riken.jp.

0166-4328/$ – see front matter © 2010 Elsevier B.V. All rights reserved.
doi:10.1016/j.bbr.2010.04.037

Table 1
Summary of conditioning schedule.

	Conditioning 1	Conditioning 2	Test
Group CN	No treatment	Context + noise	Noise
Group C-CN	Context	Context + noise	Noise
Group CC	Context	Context	Noise
Group LN	No treatment	Light + noise	Noise
Group L-LN	Light	Light + noise	Noise
Group LL	Light	Light	Noise

Note: Noise was 70 dB of broadband white noise. Light was supplied by white LED (150 lx).

blocking experiment is explicit, the "memory" that inhibits the later CS-US learning in latent inhibition is implicit. This fact suggests that blocking and latent inhibition may reflect different neuronal mechanisms. The aim of this study was to develop a simple procedure for examining the blocking effect in mice, and to evaluate the performance of this procedure in mouse strains commonly used in behavioral experiments in order to develop a new animal model of mental disorders.

Subjects included 48 male C57BL/6J mice, 21 male DBA/2J mice, and 20 male ICR mice. All mice were commercially obtained (JCL Inc., Tokyo, Japan) at 8 weeks of age and were housed individually for 1 week prior to the experiment. The breeding room and experimental room were air-conditioned (22 °C, 50–60% humidity), and a 12-h light–dark cycle was implemented (lights on at 08:00). Food and water were freely available except during experimentation. All experiments were conducted during the light cycle, between 13:00 and 17:00. All animal experiments in this study were performed in strict accordance with the guidelines of The Institute of Physical and Chemical Research (RIKEN), and were approved by the institute's Animal Investigation Committee.

Experimental apparatuses consisted of two types of sound-proof boxes (40 cm × 50 cm × 60 [H] cm each; inside wall white or black), a shock chamber (10 cm × 10 cm × 10 [H] cm; clear Plexiglas with 2-mm-diameter stainless steel shock grids), a test chamber (10 cm × 10 cm × 10 [H] cm; clear Plexiglas without shock grids), and a shock generator and scrambler (O'Hara, Tokyo, Japan). The ceiling of each sound-proof box was equipped with a fluorescent bulb (white box; 4 W; ~70 lx on the floor of the box) or light-emitting diodes (LED; black box; ~90 lx on the floor of the box). In addition, two LEDs (for CS; ~150 lx) were placed on the side walls of the black box. Experiments were controlled by a Macintosh computer and data were collected and analyzed using Image FZ software (O'Hara) modified from NIH Image (free software available at http://rsb.info.nih.gov/nih-image/).

Mice were randomly divided into three groups, as summarized in Table 1. The first group received only context and cued conditioning (classical fear conditioning) on day 2 (group CN). The second group received a series of contextual conditioning on day 1 and classical fear conditioning on day 2 (group C-CN). The final group received a series of contextual conditioning on day 1 and another contextual conditioning on day 2 (group CC). In the contextual conditioning, there was no obvious stimulus except the inside of the sound-proof box and experimental chamber. In contrast, in the context and cued conditioning trial, three 15-s pulses of white noise (70 dB) were presented as CS, each followed by a foot shock (0.3 mA, 2 s). In the first contextual conditioning of group C-CN and group C-C, eight foot shocks (0.3 mA, 2 s each) were administered at 1-min intervals without noise presentation. In the second contextual conditioning of group C-C, mice were given three foot shocks (0.3 mA, 2 s each) at 1-min intervals. On day 3, a test trial was conducted for all groups. Mice were individually introduced to a test chamber that was a completely different environment from that of the conditioning chamber. The two-part test trial consisted of 2 min for assessing the non-specific fear response to the new environment, followed

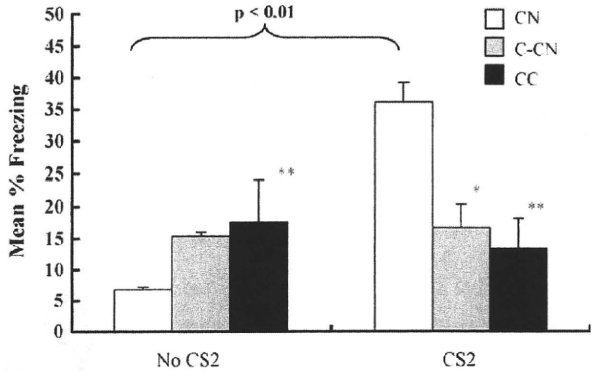

Fig. 1. Context-noise conditioning in C57BL/6J mice ($n = 9$ in each group). Data represent mean + SEM. Group names are described in the text. CS2 was white noise. Asterisks indicate statistical significance compared to CN (*$p < 0.05$; **$p < 0.01$).

by 2 min for assessing the fear response to the white-noise CS. In C57BL/6J mice, a light CS experiment (150 lx, 15 s) was conducted in addition to the noise CS experiment. Fear response was assessed by freezing rate, which was calculated as freezing rate = (no movement time/duration of experiment) × 100.

Fig. 1 shows the results of the C57BL/6J white-noise CS experiment. In the first 2 min (left; no CS2), one-way ANOVA revealed a significant conditioning effect ($F(2,24) = 10.69$, $p < 0.001$), and post-hoc analysis (Turkey's test) showed that the freezing rate of group CC was statistically higher than that of group CN ($T = 6.45$, $p < 0.01$). This enhanced fear response in group CC was a non-specific fear response caused by repeated contextual conditioning over 2 consecutive days. In the second 2 min (right; CS2), one-way ANOVA again revealed a significant conditioning effect ($F(2,24) = 7.34$, $p < 0.01$), and post-hoc analysis (Turkey's test) showed that the freezing rates of groups C-CN and CC were both statistically lower than that of group CN ($T = 4.29$, $p < 0.05$ and $T = 5.03$, $p < 0.01$, respectively). Within-group comparisons revealed a significant statistical difference only in group CN ($T = 2$, $p < 0.01$, Wilcoxon's test). These results indicate that conditioning prior to the contextual CS may block subsequent conditioning to another CS (white noise).

Fig. 2 shows the results of the C57BL/6J light CS experiment. In the first 2 min (left; no CS2), one-way ANOVA revealed no significant conditioning effect ($F(2,21) = 1.57$, n.s.). These results indicate that there was no enhanced non-specific fear response in either group following CS conditioning with light. In the second 2 min

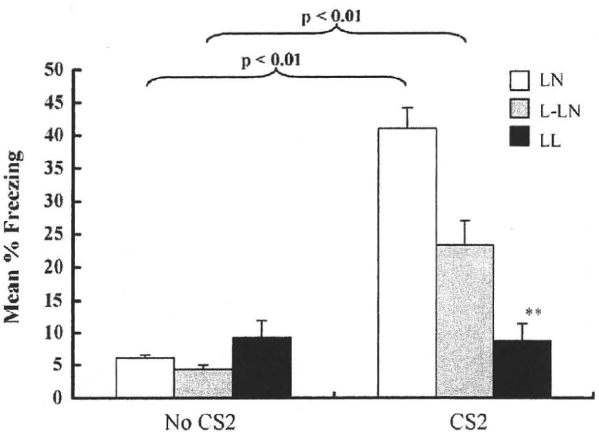

Fig. 2. Context-light conditioning in C57BL/6J mice ($n = 7$ in each group). Data represent mean + SEM. Group names are described in the text. CS2 was light stimulus. Asterisks indicate statistical significance compared to LN (**$p < 0.01$).

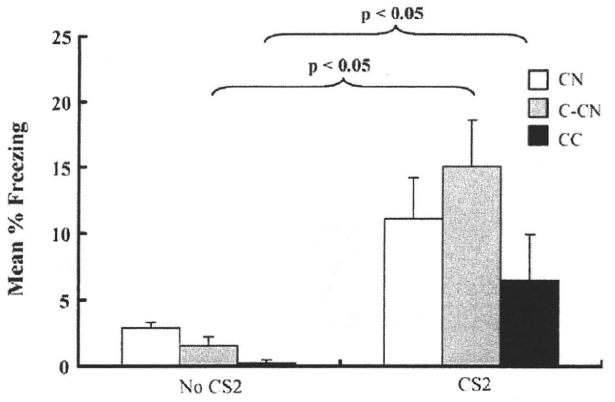

Fig. 3. Context-noise conditioning in DBA/2J mice ($n = 7$ in each group). Data represent mean + SEM. Group names are described in the text. CS2 was white noise.

(right; CS2), one-way ANOVA revealed a significant conditioning effect ($F(2,21) = 9.31$, $p < 0.005$), and post-hoc analysis (Turkey's test) showed that the freezing rate of group LL was statistically lower than that of group LN ($T = 6.09$, $p < 0.01$), but the freezing rate of group L-LN was not significantly lower than that of group LN. Within-group comparisons revealed statistical differences in groups LN and L-LN ($T = 0$, $p < 0.01$ and $T = 0$, $p < 0.01$, respectively; Wilcoxon's test). These results indicate that repeated conditioning to the light CS used in this study produced only an incomplete blocking effect.

Fig. 3 shows the results of the tone CS experiment using an inbred mouse strain, DBA/2J. In the first 2 min (left; No CS2), because an initial Bartlett's test was significant, ANOVA could not be applied, so a non-parametric test (Steel Dwass's test) was conducted. This test showed that there were no statistical differences between groups. In the second 2 min (right; CS2), one-way ANOVA revealed no significant conditioning effect ($F(2,18) = 0.99$, n.s.). Within-group comparisons revealed statistical differences in groups C-CN and CC ($T = 0$, $p < 0.05$ and $T = 0$, $p < 0.05$, respectively; Wilcoxon's test). These results indicate that DBA/2J mice can easily learn certain types of classical fear conditioning but did not exhibit any blocking effect, at least in this protocol.

Finally, Fig. 4 shows the results of the tone CS experiment using ICR mice. In the first 2 min (left; no CS2), as for DBA/2J mice, the initial Bartlett's test was significant, but subsequent analysis by Steel Dwass's non-parametric test revealed no statistical differences. In the second 2 min (right; CS2), one-way ANOVA revealed no significant conditioning effect ($F(2,17) = 2.52$, n.s.). However, within-group comparisons revealed statistical differences in all groups (CN: $T = 0$, $p < 0.05$; C-CN: $T = 9$, $p < 0.05$; CC: $T = 0$, $p < 0.05$; Wilcoxon's test). These results indicate that ICR mice can learn classical fear conditioning, but the context CS did not block the response to the noise CS under these experimental conditions.

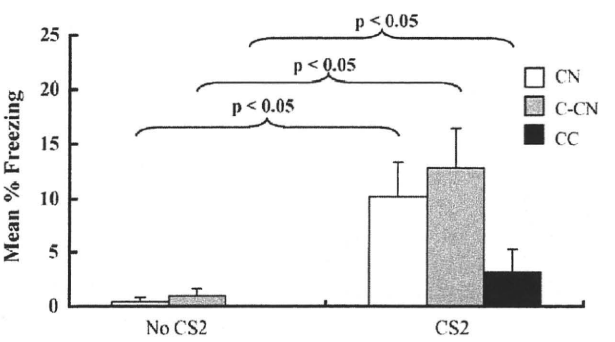

Fig. 4. Context-noise conditioning in ICR mice ($n = 7$ in group CN and C-CN, $n = 6$ in group CC). Data represent mean + SEM. Group names are described in the text. CS2 was white noise.

In this study, a simple blocking experiment for mice was developed and tested using several commonly used laboratory mouse strains. To simplify the methodology, a conventional classical fear conditioning protocol was used, and a successful blocking effect was obtained in the C57BL/6J strain, which has been widely used in learning and memory experiments and is the background strain for many genetically modified mice [5]. In contrast, DBA/2J and ICR mice only exhibited cued (auditory) fear conditioning, and did not exhibit any blocking effects. These results suggest that there are strain differences in the blocking effect using contextual conditioning. Therefore, studies of selective attention using a contextual blocking procedure should be conducted in the C57BL/6J strain and genetically modified mice of C57BL/6J background.

In the present protocol, multiple foot shocks were presented to mice in the first contextual conditioning phase (groups C-CN, CC, L-LN, and LL). Previous studies reported that inescapable foot shock could lead to learning deficits (e.g., learned "helplessness") [19]. Although multiple inescapable foot shocks were presented to the mice in this study, none of the mice in any strain displayed "helplessness" (being unable to learn second conditioning and/or immobile) and all strains were able to learn auditory-cued conditioning. Furthermore, all mice could explore freely in the cage, both with and without white-noise presentation (data not shown). These observations indicate that mice were able to learn in this procedure, and that the test can be used fairly to assess the blocking effect in mice.

Recently, latent inhibition has been used to assess functional properties of mutant mice [14,20]. Because mice are left only in the conditioning chamber, this procedure may be simpler than the blocking method. However, latent inhibition reflects the effect of implicit learning (CS evokes no events) on later conditioning, whereas blocking reflects the effect of explicit events (CS evokes foot shock) on later conditioning. This difference likely underlies different mechanisms for these two phenomena. Therefore, it may be better to apply both methods to the analysis of selective attention mechanisms in mice.

The three mouse strains used in this study (C57BL/6J, DBA/2J, and ICR) have been used in many behavioral studies and their behavioral properties have been well characterized [4]. Although C57BL/6J mice have often been reported to have hearing deficits, such hearing deficit progresses slowly over a year [23]. In this study, mice were 8 weeks of age at the beginning of the experiment, so their auditory abilities were intact. Hearing deficits in DBA/2J mice more rapidly progress than in C57BL/6J mice [23], but these mice still maintain their hearing ability until at least 6 months. Thus, no effect of hearing loss should confound the results of the current study. DBA/2J mice have also been reported to have learning deficits in trace fear conditioning [8]. However, a delayed conditioning procedure was used in this study, and these mice successfully learned auditory fear conditioning. Therefore, the hearing and/or learning deficiency in DBA/2J mice seem unlikely to have affected this results. DBA/2J mice learned the fear-conditioned response to the auditory CS but did not exhibit any blocking effect in the test phase. As the freezing rate of DBA/2J mice was almost identical to that of C57BL/6J mice, the absence of a blocking effect might be attributable to lower attention to the contextual stimuli in DBA/2J mice. A recent study reported that DBA/2J mice showed schizophrenia-like endphenotypes, including impaired latent inhibition [21]. In the present study, DBA/2J mice did not exhibit blocking. Taken together, these results suggest that the DBA/2J strain may be, a useful animal model of human mental disorders. Like DBA/2J mice, ICR mice displayed a normal but lower auditory fear-conditioned response and exhibited no contextual

blocking effects to the white-noise CS (group C-CN). Nevertheless, the absence of a blocking effect might be attributed not only to lower attention to the contextual stimuli but also to their higher activity in the test cages than other strains (data not shown).

The results of the present study indicate that mice, especially of the C57BL/6J strain, can be used to assess selective attention (blocking). In so doing, I have demonstrated that mice have the capacity for selective attention and can be used as an animal model of selective attention. Furthermore, the method described herein can be applied to the analysis of genetically engineered mice that lack the blocking effect, which can serve as an animal model of mental disorders such as schizophrenia. Application of the present protocol to the analysis of genetically engineered mice will further our understanding of the mechanisms underlying selective attention.

Acknowledgement

This study was supported in part by the Ministry of Health, Labour and Welfare (Tokyo, Japan; H20-Chemistry-General-009).

References

[1] Anscombe R. The disorder of consciousness in schizophrenia. Schizophr Bull 1987;13:241–60.
[2] Bender S, Muller B, Oades RD, Sartory G. Conditioned blocking and schizophrenia: a replication and study of the role of symptoms, age, onset-age of psychosis and illness-duration. Schizophr Res 2001;49:157–70.
[3] Cherry EC. Some experiments on the recognition of speech, with one and with two ears. J Acoust Soc Am 1953;25:975–9.
[4] Crawley JN. Behavioral phenotyping strategies for mutant mice. Neuron 2008;57:809–18.
[5] Crawley JN, Belknap JK, Collins A, Crabbe JC, Frankel W, Henderson N, et al. Behavioral phenotypes of inbred mouse strains: implications and recommendations for molecular studies. Psychopharmacology (Berl) 1997;132:107–24.
[6] Crookes AE, Moran PM. An investigation into age and gender differences in human Kamin blocking, using a computerized task. Dev Neuropsychol 2003;24:461–77.
[7] Escobar M, Oberling P, Miller RR. Associative deficit accounts of disrupted latent inhibition and blocking in schizophrenia. Neurosci Biobehav Rev 2002;26:203–16.
[8] Holmes A, Wrenn CC, Harris AP, Thayer KE, Crawley JN. Behavioral profiles of inbred strains on novel olfactory, spatial and emotional tests for reference memory in mice. Genes Brain Behav 2002;1:55–69.
[9] Jones SH, Gray JA, Hemsley DR. Loss of the Kamin blocking effect in acute but not chronic schizophrenics. Biol Psychiatr 1992;32:739–55.
[10] Jones SH, Hemsley DR, Ball S, Serra A. Disruption of the Kamin blocking effect in schizophrenia and in normal subjects following amphetamine. Behav Brain Res 1997;88:103–14.
[11] Kamin LJ. Predictability, surprise, attention, and conditioning. In: Campbell BA, Church RM, editors. Punishment and aversive behavior. New York: Appleton-Century-Crofts; 1969. p. 279–96.
[12] Mackintosh NJ. A theory of attention: variations in the associability of stimuli with reinforcement. Psychol Rev 1975;82:276–98.
[13] Mirsky AF, Duncan CC. Etiology and expression of schizophrenia:neurobiological and social factors. Ann Rev Psychol 1986;37:291–319.
[14] Miyakawa T, Leiter LW, Gerber DJ, Gainetdinov RR, Sotnikova TD, Zeng H, et al. Conditional calcineurin knockout mice exhibit multiple abnormal behaviors related to schizophrenia. Proc Natl Acad Sci USA 2003;100:8987–92.
[15] Moran PM, Al-Uzri MM, Watson J, Reveley MA. Reduced Kamin blocking in non paranoid schizophrenia: associations with schizotopy. J Psychiatr Res 2003;37:155–63.
[16] Moran PM, Owen L, Crookes AE, Al-Uzri MM, Reveley MA. Abnormal prediction error is associated with negative and depressive symptoms in schizophrenia. Prog Neuropsychopharmacol Biol Psychiatry 2008;32:116–23.
[17] Ohad D, Lubow RE, Weiner I, Feldon J. The effects of amphetamine on blocking. Psychobiology 1987;15:137–43.
[18] O'Tuathaigh CM, Salum C, Young AM, Pickering AD, Joseph MH, Moran PM. The effect of amphetamine on Kamin blocking and overshadowing. Behav Pharmacol 2003;14:315–22.
[19] Seligman ME. Learned helplessness. Annu Rev Med 1972;23:407–12.
[20] Shen S, Lang B, Nakamoto C, Zhang F, Pu J, Kuan S-L, et al. Schizophrenia-related neural and behavioral phenotypes in transgenic mice expressing truncated Disc1. J Neurosci 2008;28:10893–904.
[21] Singer P, Feldon J, Yee BK. Are DBA/2 mice associated with schizophrenia-like endophenotypes? A behavioural contrast with C57BL/6 mice. Psychopharmacology 2009;206:677–98.
[22] Suiter RD, LoLordo VM. Blocking of inhibitory Pavlovian conditioning in the conditioned emotional response procedure. J Comp Physiol Psychol 1971;76:137–44.
[23] Turner JG, Parrish JL, Hughes LF, Toth LA, Caspary DM. Hearing in laboratory animals: strain differences and nonauditory effects of noise. Comp Med 2005;55:12–23.
[24] Yamada K. Application of gene-engineered mice to the development of a new model animal of stress-induced mental disorders. Jap J Anim Psychol 2004;54:41–7.
[25] Yamada K, Wada K. Animal models of schizophrenia—application of gene-targeted animals. Schizophr Front 2004;5:143–7.

GLIA

GLIA 58:1197–1207 (2010)

Glycosphingolipid Synthesis in Cerebellar Purkinje Neurons: Roles in Myelin Formation and Axonal Homeostasis

SHUN WATANABE,[1,2,3] SHOGO ENDO,[4] ERIKO OSHIMA,[1] TOMIKO HOSHI,[5,6] HIDEYOSHI HIGASHI,[3] KAZUYUKI YAMADA,[8] KOUJIRO TOHYAMA,[6] TADASHI YAMASHITA,[7] AND YOSHIO HIRABAYASHI[1,2]*

[1]*Laboratory for Molecular Membrane Neuroscience, Brain Science Institute, RIKEN, Wako-Shi, Saitama, Japan*

[2]*CREST, Japan Science and Technology Agency, Kawaguchi-Shi, Saitama, Japan*

[3]*Division of Glyco-signal Research, Institute of Molecular Biomembrane and Glycobiology, Tohoku Pharmaceutical University, Sendai-Shi, Miyagi, Japan*

[4]*Aging Regulation Team, Tokyo Metropolitan Institute of Gerontology, Itabashi-Ku, Tokyo, Japan*

[5]*Support Unit for Neuromorphological Analysis, Research Resources Center, Brain Science Institute, RIKEN, Wako-Shi, Saitama, Japan*

[6]*The Center for EM and Bio-Imaging Research, Nano-Neuroanatomy, Iwate Medical University, Morioka-Shi, Iwate, Japan*

[7]*Graduate School of Life Science, Hokkaido University, Sapporo-Shi, Hokkaido, Japan*

[8]*Support Unit for Animal Experiment, Research Resources Center, Brain Science Institute, RIKEN, Wako-Shi, Saitama, Japan*

KEY WORDS
glycolipid; glucosylceramide; glycosyltransferase; myelination; Purkinje neuron

ABSTRACT
Glycosphingolipids (GSLs) occur in all mammalian plasma membranes. They are most abundant in neuronal cells and have essential roles in brain development. Glucosylceramide (GlcCer) synthase, which is encoded by the *Ugcg* gene, is the key enzyme driving the synthesis of most neuronal GSLs. Experiments using conditional Nestin-Cre *Ugcg* knockout mice have shown that GSL synthesis *in vivo* is essential, especially for brain maturation. However, the roles of GSL synthesis in mature neurons remain elusive, since Nestin-Cre is expressed in neural precursors as well as in postmitotic neurons. To address this problem, we generated Purkinje cell-specific *Ugcg* knockout mice using mice that express Cre under the control of the L7 promoter. In these mice, Purkinje cells survived for at least 10–18 weeks after *Ugcg* deletion. We observed apparent axonal degeneration characterized by the accumulation of axonal transport cargos and aberrant membrane structures. Dendrites, however, were not affected. In addition, loss of GSLs disrupted myelin sheaths, which were characterized by detached paranodal loops. Notably, we observed doubly myelinated axons enveloped by an additional concentric myelin sheath around the original sheath. Our data show that axonal GlcCer-based GSLs are essential for axonal homeostasis and correct myelin sheath formation.

INTRODUCTION

Glycosphingolipids (GSLs) form lipid microdomains (rafts) that serve as key assembly and sorting platforms for cell–cell interactions and signal transduction complexes. They are also involved in the regulation of multiple cellular processes. Glucosylceramide (GlcCer) is the core precursor molecule of most GSLs, which have many different carbohydrate chains. Some GSLs (e.g., gangliosides) even contain sialic acids. GlcCer synthesis is catalyzed by glucosyltransferase, which is encoded by the *Ugcg* gene (Ichikawa and Hirabayashi, 1998). In addition, a few GSLs that are characteristic components in myelin are derived from galactosylceramide.

Previous studies have suggested that GSLs play an important role in neural cells for processes such as axonal elongation (Boldin and Futerman, 1997; Mutoh et al., 1998; Schwarz and Futerman 1997); synaptic transmission (Fujii et al., 2002); and neuron-glia interactions (Vyas et al., 2002). To elucidate their physiological functions *in vivo*, researchers have generated ganglioside synthase gene knockout (KO) mice. Disruption of the mouse *Ugcg* gene results in embryonic lethality during gastrulation, demonstrating an essential role of the *Ugcg* gene in embryo survival (Yamashita et al., 1999). Mice lacking complex gangliosides reach adulthood with nervous system deficits (Inoue et al., 2002; Sheikh et al., 1999; Sugiura et al., 2005; Yamashita et al., 2005b). Jennmann et al. (2005) also generated neural cell-specific disruption of the *Ugcg* gene using a Nestin-Cre transgenic deleter strain. These mice displayed neuronal defects and died between postnatal Days 11 and 24, suggesting that GSLs are required for brain maturation after birth. Compared with mice lacking complex gangliosides, Jennmann et al.'s *Ugcg* knockout mice have a severe phenotype, emphasizing the importance of GlcCer-based GSLs in the nervous system. However, because GSL synthesis was suppressed in both neuronal and non-neuronal cells, such as radial glia, it is unclear

Additional Supporting Information may be found in the online version of this article.

Grant sponsors: Grant-in-Aid for Strategic Medical Science Research Center, Ministry of Education, Culture, Sports, Science and Technology of Japan, 2009-2013; CREST of JST (Japan Science and Technology Agency).

*Correspondence to: Yoshio Hirabayashi, Laboratory for Molecular Membrane Neuroscience, Brain Science Institute, RIKEN, 2-1 Hirosawa, Wako-shi, Saitama 351-0198, Japan. E-mail: hirabaya@riken.jp

Received 16 October 2009; Accepted 10 March 2010

DOI 10.1002/glia.20999

Published online 9 April 2010 in Wiley InterScience (www.interscience.wiley.com).

whether the observed axonal dystrophy and neurodegeneration represented neuron-autonomous defects. Since neighboring non-neuronal cells such as astrocytes and oligodendrocytes support neuronal cell survival and function, glial-expressed GSLs might influence neurons indirectly, via neuronal-glial interactions; for example, GSLs on astrocytes can affect axonal elongation (Freire et al., 2004). In addition, the short survival time of Nestin-Cre-driven conditional *Ugcg* KO mice precludes the examination of GlcCer-based GSL function at adult stages.

In this study, we generated Purkinje cell-specific *Ugcg* KO mice by crossing L7 gene promoter-driven *Cre* transgenic mice and *Ugcg*-flanked mice. In the cerebellum of *L7-Cre* : $Ugcg^{loxP/loxP}$ mice, Cre expression was specific to Purkinje cells three weeks after birth, when most Purkinje cells have already matured. We observed dystrophic morphology of Purkinje cell axons and subsequent degeneration. Furthermore, our histological analyses demonstrated that axonal transport cargos abnormally accumulated in swollen axons, suggesting that axonal transport was impaired in *Ugcg* (−/−) neurons. These mice displayed an unusual myelin morphology in which some axons were "doubly myelinated," having what appeared to be an additional compact myelin sheath completely enveloping the original myelin sheath. Our results suggested that *de novo* synthesis of GSLs in neurons is essential for the maintenance of axonal homeostasis and normal myelin formation.

MATERIALS AND METHODS

Transgenic Animals

Mice with loxP-flanked exons 7-9 of the *Ugcg* gene locus were generated as described (Yamashita et al., 2005a). For the generation of mice with a Purkinje cell-specific deletion of *Ugcg*, homozygous floxed mice were crossed with homozygous *L7-Cre* mice to generate double-heterozygous offspring. These were intercrossed to yield $Ugcg^{loxP/-}$: $L7\text{-}Cre^{tg/tg}$ mice, which were finally crossed with $Ugcg^{loxP/loxP}$ mice to yield $Ugcg^{loxP/loxP}$: $L7\text{-}Cre^{tg/0}$ mice for analysis (Fig. 1A). These mice appeared in the expected Mendelian ratio of around 50% of the litters. Their $Ugcg^{loxP/-}$: $L7\text{-}Cre^{tg/0}$ littermates were used as controls in each experiment.

Genotyping of Mutant Mice

PCR analysis of tail biopsies was performed for confirmation of the wild-type, floxed, and null alleles (Fig. 1A). For PCR, the following primers were used: Ugcg/wild type forward (primer 1; Fig. 1A), 5′-ATGTGCTAGATCAGGCA GGAGGGCTCATAG-3′; wild type/Ugcg-flox reversed (primer 2), 5′-CCAACAGATATTGAATGCGAATGCTCTG CC-3′; Ugcg null reversed (primer 3), 5′-GAGCCAGTCC ATTACTCTCGTTGATTGCAT-3′. PCR products of about 230 bp, 280 bp, and 300 bp were indicative of the wild-type, floxed, and null alleles, respectively (Yamashita et al., 2005a). The constitutive L7Cre transgene was detected using the following primers: L7Cre forward, 5′-AGGTTCGTTCACTCATGGA-3′; and L7Cre reverse, 5′-TCGACCAGTTTAGTTACCC-3′. A 200 bp PCR product was indicative of the L7Cre transgene.

Immunohistochemistry and Fluorescent Light Microscopy

Adult mice were anesthetized with 0.1 mL of 50 mg/mL Nembutal. They were perfusion-fixed with 4% (w/v) paraformaldehyde (PFA) in 0.1 M phosphate buffer, pH 7.4,

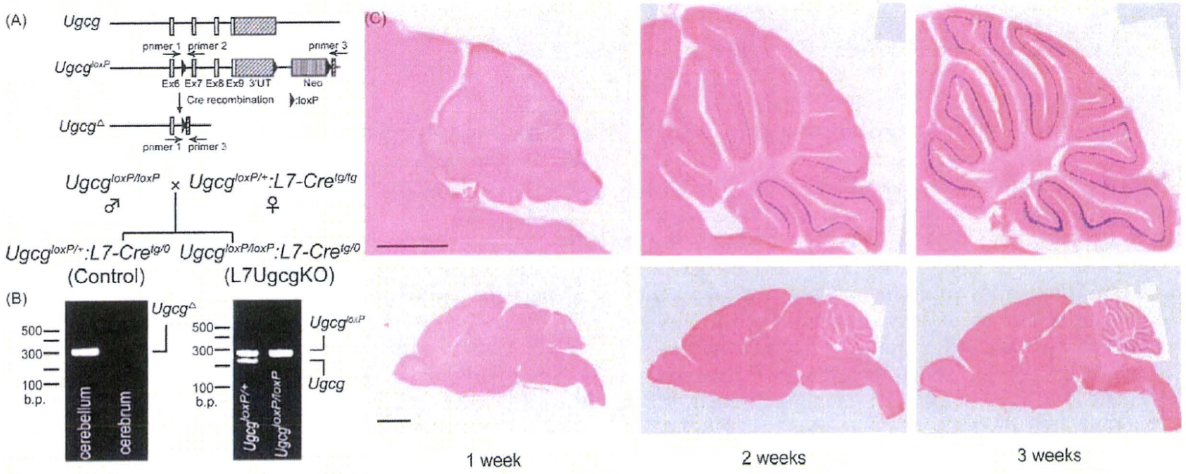

Fig. 1. Generation and characterization of floxed allele. **A**: Schematic representation of Cre-mediated recombination of $Ugcg^{loxP}$. The predicted outcome of Cre recombination is shown at the bottom. **B**: Identification of Cre-mediated recombination of the $Ugcg^{loxP}$ allele in brain (left panel). Genomic DNA from cerebellum and cerebrum of 8-week-old L7UgcgKO mice were subjected to PCR analysis using primers 1 and 3. Identification of the $Ugcg^{loxP}$ allele (right panel). Tail DNA from $Ugcg^{loxP/+}$; $L7\text{-}Cre^{tg/0}$ and $Ugcg^{loxP/loxP}$: $L7\text{-}Cre^{tg/0}$ mice were subjected to PCR analysis using primers 1 and 2. **C**: An L7-Cre mouse was bred with a Rosa26-lacZ reporter mouse, and Cre expression in the cerebellum of the resulting progeny was assessed for β-galactosidase activity. In the sagittal sections from mice 1–3 postnatal weeks old, blue-colored staining indicates Purkinje cell-specific Cre expression. Scale bars: 2 mm (lower panels); 1 mm (upper panels).

using a peristaltic pump. The perfused brain tissues were post-fixed in 4% PFA in 0.1 M phosphate buffer overnight at 4°C and embedded in 5% low-melting agarose gel. Sagittal sections of the cerebellum were cut at 50 μm using a LEICA microtome and stored in phosphate-buffered saline (PBS) at 4°C. In a few cases cerebellar coronal sections were cut. Free-floating sections of cerebellum were blocked for non-specific binding with PBS containing 0.1% (v/v) Triton X-100 and 10% (v/v) goat serum and incubated with primary antibody at 4°C overnight. The sections were washed and incubated with a species-appropriate secondary antibody (AlexaFluor-conjugated anti-rabbit, antirat, or anti-mouse IgG) at room temperature for 120 min, washed extensively, mounted onto glass slides with Immu-mount (Shandon, Inc., Pittsburgh, PA), and examined with fluorescent light microscopes. For some sections, cell nuclei were counterstained with 4′,6′-diamidino-2-phenylindole (DAPI; Nacalai Tesque Inc., Kyoto, Japan). For sodium channel and Caspr staining, PFA-perfused brains were cryoprotected with 30% sucrose in PBS (pH 7.4) for 24 h at 4°C, as described previously (Hoshi et al., 2007). After embedding in optimal cutting temperature (OCT)-mounting medium, the blocks were cut in 8-μm-thick sections.

For hematoxylin and eosin (HE) staining, PFA-perfused brains were kept in the same PFA fixative solution for one week, and then embedded in paraffin. Paraffin-embedded brains were sectioned at a thickness of 5 μm and processed for H&E staining. For X-gal staining, the brains were perfused with ice-cold PBS and 30% sucrose, dissected, and rapidly frozen in mounting medium. Cryostat sections (15–20 μm) were prepared and postfixed for 5 min in 4% PFA in PBS. The fixed sections were washed and subjected to X-Gal staining overnight at room temperature. The X-Gal staining solution comprised 1 mg/mL X-Gal (4-chloro-5-bromo-3-indolyl-b-galactosidase), 4 mM $K_4Fe(CN)_6{\cdot}3H_2O$, 4 mM $K_3Fe(CN)_6$, and 2 mM $MgCl_2$ in PBS. The slides were washed with PBS twice and once in distilled water, and then counterstained with eosin.

Electron Microscopy

Animals were perfused intracardially through the left ventricle with a fixative containing 2.5% (v/v) glutaraldehyde and 2.0% (w/v) PFA in 0.1 M phosphate buffer (pH 7.4). Cerebellums were dissected and postfixed by immersion in the same fixative overnight at 4°C then sagittal 50-μm sections of the cerebellar vermis were prepared. After osmification in a 1% (w/v) osmium tetroxide solution, the specimens were dehydrated through a graded alcohol series and embedded in Epon 812 (TAAB Laboratories, Aldermaston, Berks, UK). Semithin sections were collected and stained with 0.5% (w/v) toluidine blue in 0.1 M phosphate buffer (pH 7.4). Ultrathin sections were cut using an Ultracut microtome (Leica EM-UC6) and stained with uranyl acetate and lead citrate for contrast. The sections were examined with a transmission electron microscope (Hitachi H-7100 and H-7650).

Western Blot

Cerebellar extracts were prepared in 50 mM Tris-HCl (pH 7.4), 5 mM EDTA, and one tablet of Complete mini/25 mL (protease inhibitors; Roche Diagnostics). Samples were mixed with Laemmli buffer with or without (for anti-myelin-associated glycoprotein [MAG]) 2-mercaptoethanol. SDS–PAGE was performed, and separated proteins were transferred onto polyvinylidene difluoride membranes and subjected to immunoblotting with individual primary antibodies, including anti-MAG, anti-myelin basic protein (MBP), and antialpha tubulin (internal control). Immunoreactivity was visualized with HRP-conjugated secondary antibodies and a chemiluminescence detection system, according to the manufacturer's instructions (Millipore).

Antibodies

The following primary antibodies were used: mouse monoclonal anti-cytochrome c (clone 6H2.B4); mouse anti-GM130 (BD Transduction Laboratories, San Diego, CA); mouse anti-α-tubulin; mouse antipan sodium channel; mouse antisynaptophysin (Sigma, St. Louis, MO); mouse anticalbindin D28k (Swant, Bellinzona, Switzerland); mouse anti-TuJ1 (Covance, Princeton, NJ); mouse antikinesine heavy chain; mouse anti-MAG; rabbit polyclonal anti-calbindin D28k; rabbit anti-glutamate receptor delta 1/2 (GluRδ1/2); rat anti-MBP (Chemicon International, Temecula, CA); rabbit anti-Caspr (Abcam, Cambridge, MA); and rabbit anti-GFAP (Dako). Rat anti-inositol 1, 4, 5-triphosphate receptor 1 (IP3R1, clone 18A10) antibody was kindly provided by Dr. K. Mikoshiba. Rabbit polyclonal antibody to the C terminus (amino acids 372-394) of human GlcCer synthase (GlcT-1) was generated according to Marks et al. (1999).

Statistics

Data were expressed as means ± S.E.M. Significant differences between mean values were evaluated using two-tailed, unpaired Student's *t* tests.

RESULTS

Purkinje Cell-Specific Glycosphingolipid Deletion in L7UgcgKO Mice

To ensure that Cre was exclusively expressed in Purkinje neurons, we crossed L7-Cre mice with Rosa26-lacZ reporter mice and monitored Cre expression in their double-transgenic progeny (Fig. 1C). X-Gal staining for β-galactosidase activity indicated that Cre was exclusively expressed in Purkinje neurons of adult mice. Cre expression began two weeks after birth (postmitotic stage), becoming stronger and reaching a plateau four weeks after birth. The expression was highly specific for Purkinje neurons, all of which were positive for X-gal

staining in the brains of four-week-old double transgenic mice. A similar pattern of X-gal staining was observed in cerebellar coronal sections. We detected no X-gal staining in any other neurons in the brain. However, weak signals were detectable in retina, as reported by Oberdick et al. (1990).

Ugcg$^{loxP/loxP}$: *L7-Cre*$^{tg/0}$ mice (L7UgcgKO) comprised about 50% of the litter, indicating no prenatal death (see Methods). PCR analysis detected Cre recombination in cerebellum, but not cerebrum, in 8-week-old KO mice (Fig. 1B). Immunostaining against GlcT-1 (a Golgi-localized protein) verified that the Golgi apparatus of the Purkinje cells of L7UgcgKO mice lacked GlcT-1 immunoreactivity (Fig. 2D–F, P–R). Other cells in the molecular and granule layers, however, were GlcT-1 immunoreactive (arrowheads, Fig. 2D–F, J–L). Furthermore, in contrast to control mice (*Ugcg*$^{loxP/-}$: *L7-Cre*$^{tg/0}$), in L7UgcgKO mice Purkinje cells lacked P-path antibody immunostaining (Fig. 2V–X). P-path antibody is an antibody that recognizes O-acetyl-GD3, an anabolite of glucosylceramide that is enriched in Purkinje cells (Leclerc et al., 1992). Thus, the immunohistochemical analysis confirmed the Purkinje cell-specific deletion of GlcCer synthase and absence of corresponding lipids.

Purkinje Cells With an L7-Promoted Ugcg Deletion Showed Numerous Axonal Swellings

Although the cerebellum of 22-week-old L7UgcgKO mice remained morphologically intact (Fig. 3C), Purkinje cell loss was evident (Fig. 3D,H,I), with increased GFAP expression (Supp. Info. Fig. 2). However, significant Purkinje cell loss was not observed in 14-week-old mutant mice (Fig. 3F,I), indicating that the loss of Purkinje cells occurred sometime between 14 and 22 weeks after birth. Despite Purkinje cell degeneration, 23- to 39-week-old mutant mice showed no motor deficits in an open-field test and rotor-rod test (Supp. Info. Fig. S1).

In comparison with the Purkinje cell axons of normal, age-matched mice, those of 14-week-old L7UgcgKO mice possessed numerous swellings (Fig. 4; mean ± SD swellings/section in lobule V: 14-week-old control mice, 1.0 ± 1.0; 14-week-old KO mice, 16.6 ± 5.9; 22-week-old control mice, 2.9 ± 2.3; and 22-week-old L7UgcgKO mice, 31.2 ± 10.6 swellings/section. Nine sections from three mice in each group). These swollen axons were located proximal to somata in the granular layer and were located distally in the deep cerebellar nuclei. These findings indicated that the deletion of GSLs led to axonal defects prior to Purkinje cell loss.

In contrast to the significant axonal degeneration, we did not observe dendritic degeneration in our light microscopy analysis of anticalbindin D28k immunofluorescent-stained sections (see Fig. 5). To further evaluate changes in dendrites, we examined the expression patterns of the glutamate receptor GluRδ1/2 and synaptophysin. There were no differences in localization or immunostaining intensity of either GluRδ1/2 or synaptophysin between 14-week-old control and L7UgcgKO mice (Fig. 5B,C,E,F). Thus, the *Ugcg* deletion had little effect on Purkinje cell dendrites. Apparently the *Ugcg* deletion elicits differential effects on dendritic and axonal compartments, with axons being particularly vulnerable to GSL deficiency.

Mitochondria, Synaptophysin, and Kinesin Heavy Chain Accumulate in Swollen Axons

Disruption of axonal transport causes axonal enlargement and aberrant accumulation of cargo proteins, mitochondria, and synaptic vesicles that travel to or from the axon terminal (Yagashita, 1979). To determine whether mitochondria accumulate in the swollen axons of L7UgcgKO mice, we immunostained cerebellar sections with an antibody against cytochrome c, a marker for mitochondria. The axonal swellings in L7UgcgKO mice showed enhanced cytochrome immunoreactivity compared with those in control mice (Fig. 6F), indicating that mitochondria did indeed accumulate within the axonal swellings. Furthermore, immunostaining of the synaptic vesicle protein synaptophysin and the microtubule-associated motor protein kinesin heavy chain revealed that both of these proteins also accumulated within axon swellings (Fig. 6D,E). The accumulation of these cargo molecules and organelles indicated that the mutant mice had axonal transport defects.

To further assess the effect of the GlcT-1 deletion, we examined the ultrastructure of the axonal swellings of L7UgcgKO mice. Electron microscopy revealed that the axonal swellings contained accumulated aberrant membrane structures and abnormal organelles (Fig. 6G,H). Taken together, the immunofluorescence and electron microscopy analyses show that disruption of GSLs synthesis led to axonal transport defects.

Some Axons in the Mutant Mice Were Surrounded by Two Concentric Myelin Sheaths

In L7UgcgKO mice, severe demyelination was not observed, even of swollen axons. Immunoblot analysis of cerebellar extracts revealed that myelin proteins (MBP and MAG) were present in similar amounts in control and KO mice (data not shown). In L7UgcgKO mice, however, paranodal junctions were disrupted and paranodal loops were detached from the axonal plasma membrane (Fig. 7B–D), indicating reduced adhesion between glial loops and axons.

Next, we examined Caspr localization specifically on Purkinje cell axons by co-immunostaining with IP3R1, a Purkinje cell marker (Maeda et al., 1988). Caspr was a useful marker for assessing the integrity of paranodal junctions on myelinated axons. Lengths of Caspr clusters in 17- to 22-week-old L7Ugcg KO mice were significantly shorter than those of control mice (Fig. 7E). These results are consistent with the loss of transverse bands in the paranodal loops (see Fig. 7). Furthermore, sodium channel clusters were elongated in the 17- to

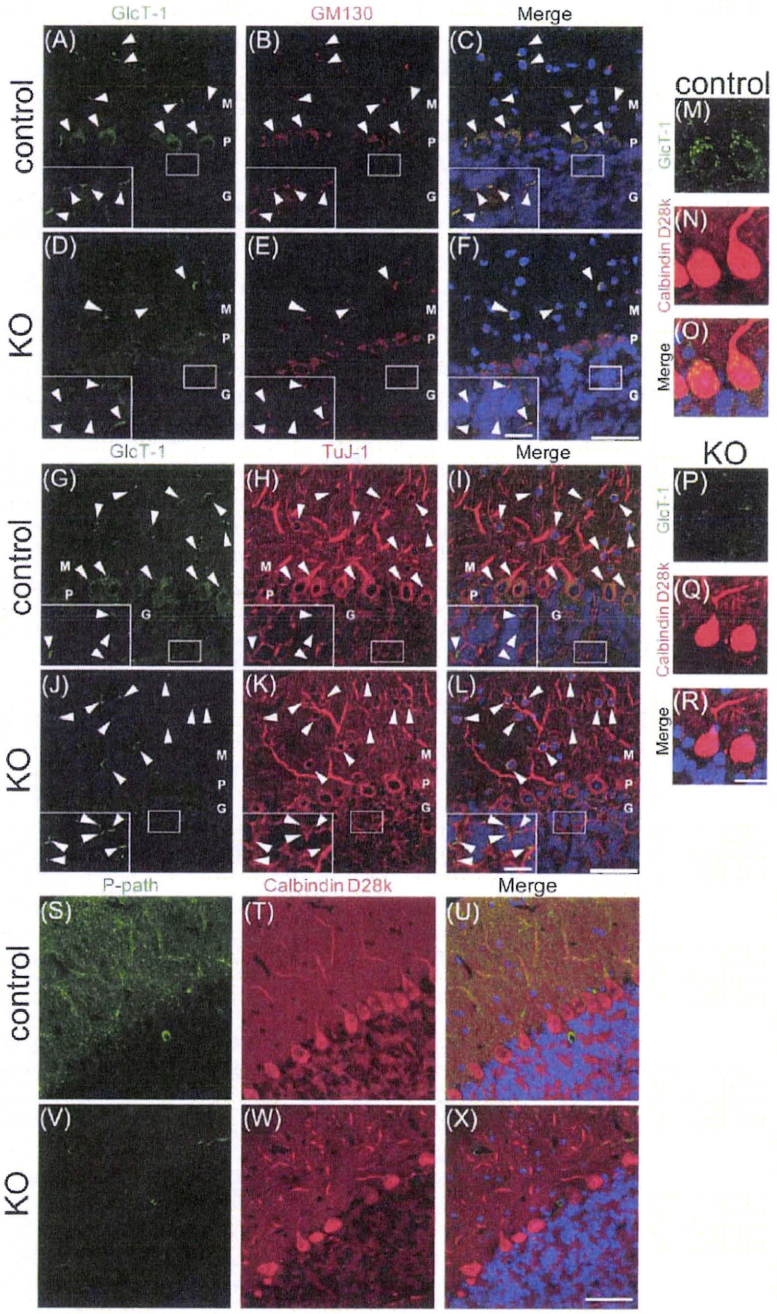

Fig. 2. Deletion of glucosylceramide synthase (GlcT-1) and an anabolite of glucosylceramide, o-acetyl GD3 (P-path antigen), were confirmed in eight-week-old Purkinje cell-specific *Ugcg* KO mice. **A–F**: Anti-GlcT-1 (A, D); anti-GM130 (Golgi apparatus marker, B,E); and merged (C,F). **G–L**: Anti-GlcT-1 (G, J); anti-TuJ-1 (neuronal marker, H, K); and merged (I, L). **M–R**: Anti-GlcT-1 (M, P); anti-calbindin D28k (N, Q); and merged (O, R). **S–X**: P-path (S, V); anti-calbindin D28k (T, W); and merged (U, X). Insets show high-magnification images of the white rectangular area in the granular layer. In the merged micrographs, cell nuclei were visualized with DAPI staining (blue). M, molecular layer; P, Purkinje cell layer; G, granule cell layer. Arrowheads point to GlcT-1-immunopostive cells. These results were observed in all mice of each genotype (n = 3). Scale bars: 50 μm (A-L, S-X); 20 μm (M-R); 10 μm (insets).

22-week-old KO mice, also suggesting disorganization of paranodal structures. These findings indicated that axonal GSLs contributed to Caspr localization and maintenance of nodal structures.

Notably, as shown in Fig. 8, excessive paranodal loops were formed on otherwise normal myelin sheaths. In longitudinally sectioned Purkinje cell axons, some myelin sheaths overlapped with neighboring sheaths and

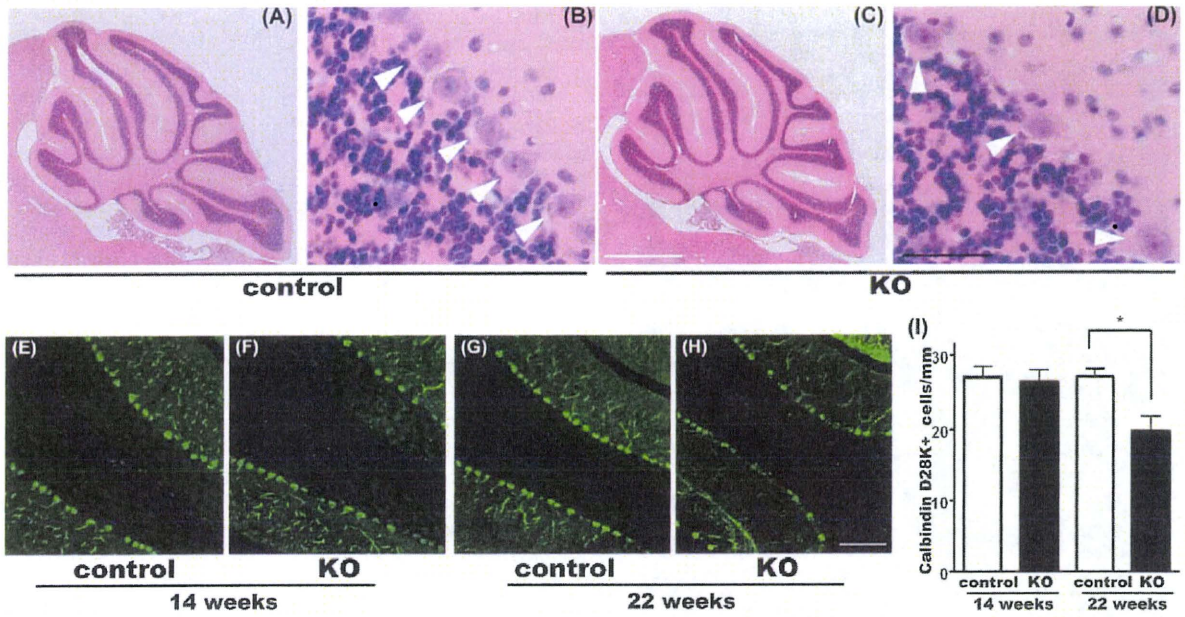

Fig. 3. Purkinje cell loss in L7UgcgKO mice. **A–D**: Hematoxylin and eosin (H&E)-stained cerebellar sections from 22-week-old control mice (A, B) and KO mice (C, D). Mid-sagittal sections through the entire extent of the cerebellum (A, C) show intact morphology in KO mice. Arrowheads point to Purkinje cell somata (B, D). Cerebellar sections from 14-week-old (**E, F**) and 22-week-old (**G, H**) control and KO mice were immunostained with anti-calbindin D28k, a Purkinje cell marker. L7UgcgKO mice showed Purkinje cell loss at 22 weeks (H), but no significant Purkinje cell loss at 14 weeks (F). Quantitation of Purkinje cells in lobule V of midsagittal sections of control and L7UgcgKO mice at 14 and 22 weeks; anticalbindin D28k stained Purkinje cells. The data are expressed as number of Purkinje cells per millimeter of Purkinje cell layer; $n = 3$, $^*P < 0.05$ (I). Scale bars: 1 mm (A, C); 50 μm (B, D); 100 μm (E–H).

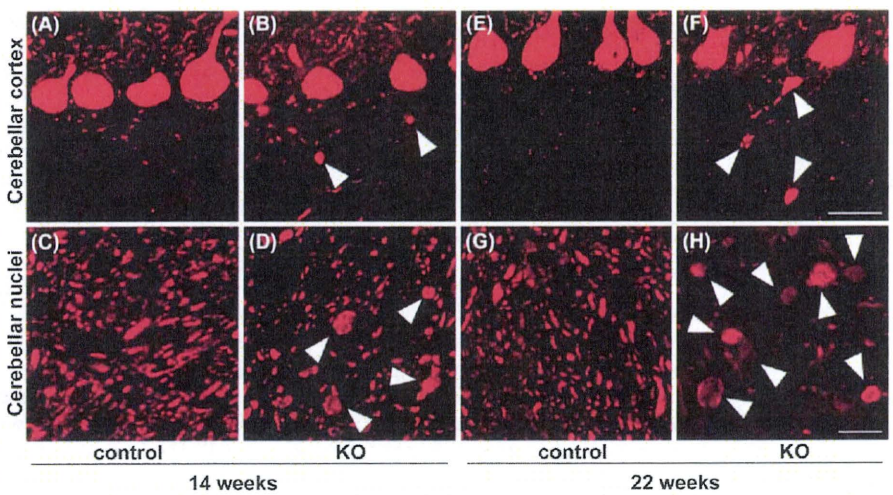

Fig. 4. Axonal swellings of Purkinje cells in L7UgcgKO mice. Cerebellar sections from 14-week-old and 22-week-old control and KO mice were immunostained with anti-calbindin D28k antibody. After postnatal week 14, axonal swellings were observed in both cerebellar deep nuclei (**D**, 14 weeks; **H**, 22 weeks) and cerebellar cortex (**B**, 14 weeks; **F**, 22 weeks). Control mice showed no axonal dystrophy in cerebellar cortex (**A**, 14 weeks; **E**, 22 weeks) or deep cerebellar nuclei (**C**, 14 weeks; **G**, 22 weeks). Arrowheads indicate axonal swellings. Scale bars: 25 μm for cerebellar cortex; 10 μm for cerebellar nuclei.

with paranodal loop-like structures that were filled with cytoplasm (see Fig. 8). Transverse bands, which link paranodal myelin loops with axolemma, were absent in these paranodal loop-like structures (Fig. 8E). These structures were observed at both postnatal 14 and 22 weeks, suggesting that the excessive paranodal loops and doubly-myelinated regions were formed prior to Purkinje cell loss.

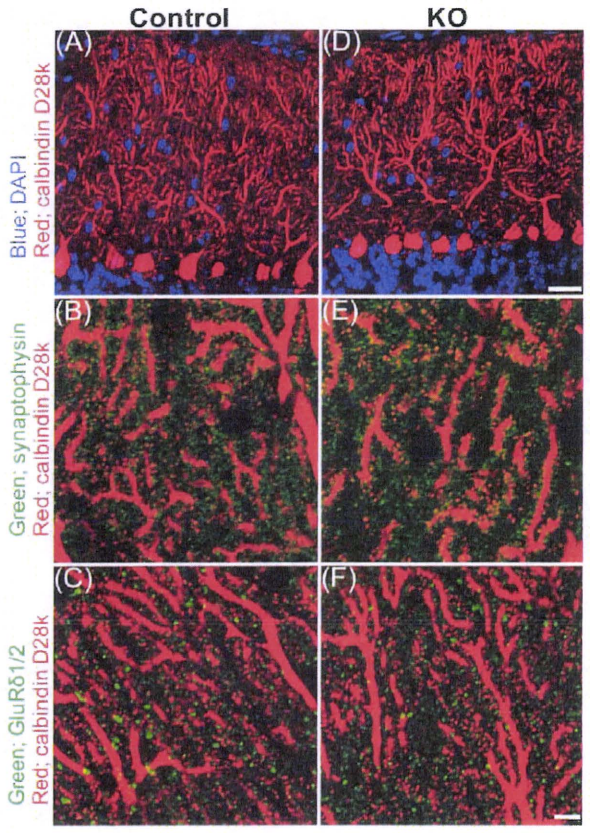

Fig. 5. *Ugcg* deletion had little effect on dendritic tree morphology. Immunofluorescent staining of cerebellar sagittal sections from 14-week-old L7UgcgKO mice showed normal localization and appearance of GluRδ and synaptophysin. The dendrites (red, ant-icalbindin D 28k immunostaining) of both wild-type and L7UgcgKO mice displayed comparable anti-synaptophysin (**B, E**; green) and anti-GluRδ1/2 (**C, F**; green) immunostaining. Nuclei were labeled with DAPI (**A, D**; blue). These results were observed in all mice of each genotype ($n = 3$). Scale bars: 50 μm for low magnification panels (A, D); 10 μm for high magnification panels (B, C, E, F).

DISCUSSION

GSLs, in particular the GlcCer-based GSLs, occur as sialic acid-containing gangliosides in the brain at a much higher concentration than in other organs. They might, therefore, play an important role in the nervous system. The majority of membrane GSLs is derived from the precursor, GlcCer. Therefore *Ugcg*, the gene encoding the glucosylceramide synthase (GlcT-1) that catalyzes the initial step of GSL biosynthesis, is a key regulator of total GSL synthesis. To elucidate the physiological roles of GSLs in neurons, we generated GlcT-1 conditional knockout mice using the Cre-loxP system. Given that GlcT-1 is essential for embryo survival, we decided to generate a Purkinje neuron-specific mutation of the *Ugcg* gene using L7-Cre transgenic mice.

In Purkinje cell-specific *Ugcg* KO mice, Purkinje cells started to degenerate 14–22 weeks after birth. This observation suggested that *Ugcg* is required for the maintenance of Purkinje cells. However, Purkinje cells survived for up to several weeks after *Ugcg* gene deletion, raising the possibility that GlcT-1 loss is not the immediate cause of the neuronal degeneration.

Before the Purkinje cell loss, we observed axonal swellings in Purkinje cells. Although axonal degeneration is considered to be diagnostic of neuronal cell death, recent studies have suggested that axonal defects are primary events that occur prior to overt neuronal degeneration following CNS injury, toxicity, genetic defects, and neurodegenerative disorders, including Alzheimer's disease (Coleman, 2005; Stokin et al., 2005). However, GlcT-1 is decreased in the brains of Alzheimer's disease patients (Marks et al., 2007), and mutant presenilin 1, which is associated with familial Alzheimer's disease, can cause the degradation of GlcT-1 protein (Mutoh et al., 2006). It is, therefore, likely that mutant presenilin 1 causes axonal defects by degrading GlcT-1 protein. Consistent with this premise is the finding that Alzheimer presenilin 1 mutations impair kinesin-based axonal transport (Lazarov et al., 2007; Pigino et al., 2003), which in turn leads to axonal swellings.

At 2.5 months of age, *St3gal5/B4galnt1* double KO mice display axonal spheroids in Purkinje cells and vacuoles in white matter (Yamashita et al., 2005b). The brains of these mice also accumulate lactosylceramide and sulfated lactosylceramide, SM3 (Yamashita et al., 2005b). Although our L7UgcgKO mice lacked all GlcCer-based GSLs, axonal swellings were not detected in 8-week-old mice (data not shown). Moreover, no vacuoles were observed in the mutant mice, even 22 weeks after birth. The relatively mild phenotype of L7UgcgKO mice compared with germline *St3gal5/B4galnt1* double-KO mice suggests that the GlcCer-based GSLs of non-neuronal cells may be essential for the maintenance of neuronal cells. Alternatively, deletion of GSLs during development may affect mature neurons at later stages. Consistent with this idea is the observation that mice in which *Ugcg* was conditionally deleted using Nestin-Cre (which is expressed during embryogenesis in the neural precursors of both neurons and glia) display more severe phenotypes (Jennemann et al., 2005), leading to neuronal degeneration and death of the mice by postnatal Day 21. These reports, together with our own findings, support the view that GSL expression during embryonic stages and/or in non-neuronal cells is required for the proper development and function of mature neurons.

In our L7UgcgKO mice, axonal swellings occurred prior to Purkinje cell loss, indicating that the axonal swellings were not secondary to neuronal degeneration. It is important to note that axonal transport defects contribute to axonal dystrophy (Coleman 2005; Stokin et al., 2005). In L7UgcgKO mice, microtubule transport cargo and machinery-such as cytochrome c, synaptophysin, and kinesin heavy chain-accumulated at axonal swellings, which is indicative of aberrant axonal transport. These observations suggest that suppression of GlcT-1 leads to axonal transport defects. Recent work indicates that cholesterol-rich microdomains are essential for synaptic vesicle sorting and that synaptic vesicle proteins are localized to cholesterol-rich microdomains (Chamber-

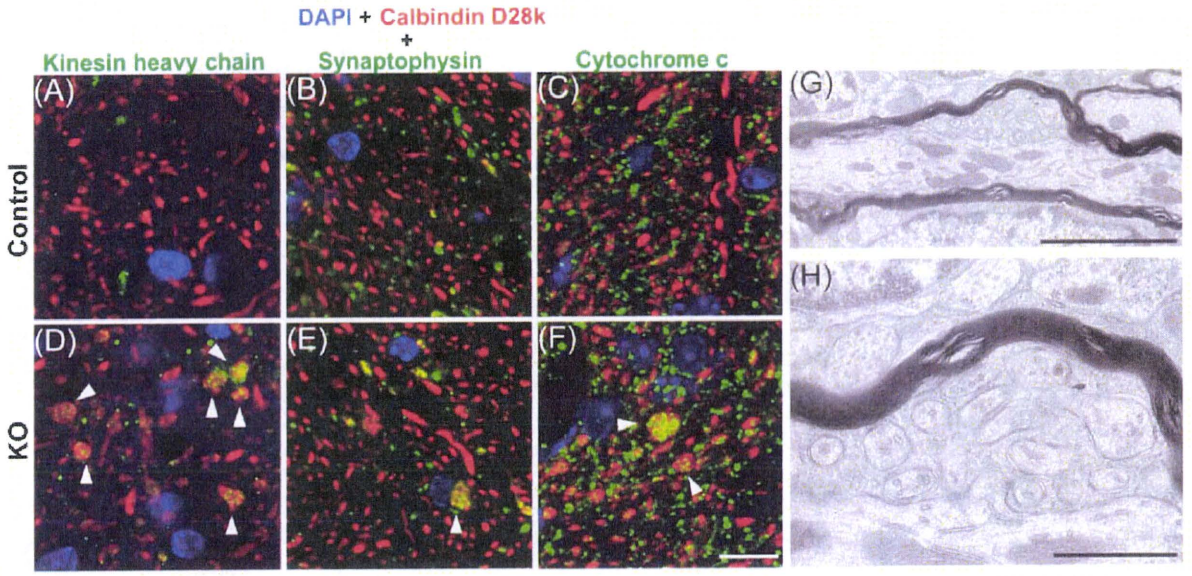

Fig. 6. Intense staining for mitochondria, synaptic vesicles, and kinesin heavy chain were observed in axonal swellings, suggesting that axonal transport was severely defective in L7UgcgKO mice. Cerebellar sections were co-immunostained with anticalbindin D28k (red) and antibodies against cargo markers (green), such as anti-kinesin heavy chain (**A, D**); antisynaptophysin (**B, E**); or anticytochrome c (**C, F**). Nuclei were labeled with DAPI (blue). Arrowheads indicate axonal swellings. Scale bar: 10 μm (A–F). Transmission electron micrograph showing the ultrastructure of a swollen axon from a L7UgcgKO mouse (**G, H**). Aberrant membrane structures and mitochondria accumulated within axonal swellings. These results were observed in all mice of each genotype (n = 3). Scale bars: 1 μm (G); 0.3 μm (H).

lain et al., 2001). Cholesterol/sphingolipid or GM1/cholera toxin B subunit complexes enhance microtubule-associated kinesin motor motility (Klopfenstein et al., 2002). The axonal swellings observed in our KO mice may be due to microdomain disruption, since GSLs and cholesterol are major components of lipid microdomains.

On the other hand, axonal degeneration and myelin disorganization are closely related. Although we did not detect severe demyelination in L7UgcgKO mice, their paranodal junctions were malformed, having shorter Caspr clusters. Caspr mutant mice develop paranodal disruptions and axonal swellings accompanied by mitochondria accumulation and cytoskeletal disorganization (Garcia-Fresco et al., 2006). Thus, abnormal localization of Caspr in L7UgcgKO mice may result in axonal swellings.

Disruption of paranodal junctions was also observed in germline *B4galnt1* KO mice and *St3gal5/B4galnt1* double-null mice (Susuki et al., 2007; Yamashita et al., 2005b). Unlike these KO mice, which lack GSLs in both axons and myelin, our L7UgcgKO mice only lack axonal GSLs. Thus, axonal GSLs are definitely essential for maintaining axo-glial interactions at paranodal junctions and for proper attachment of paranodal loops on the axolemma with transverse bands in conjunction with other cell adhesion molecules. On the other hand, because some membrane proteins are localized in lipid rafts, deleting axonal GSLs might impair lipid raft-dependent interactions between axonal membranes and oligodendrocyte processes. Supporting this idea are the findings that GlcCer-based GSLs in axons and/or oligodendrocytes contribute to localization of Caspr, an axonal adhesion molecule, in lipid microdomain/lipid rafts at the paranodal junction (Susuki et al., 2007). Indeed, the disrupted axo-glial interactions exhibited by *Ugt8*- or *Gal3st1*-mutant mice further support the premise that GalCer-based GSLs, which are enriched in myelin, play important roles in the maintenance of paranodal structures and Caspr localization (Dupree et al., 1999; Hoshi et al., 2007). Additionally, *Ugt8*-KO mice also show significant reduction of raft-associated Caspr (Schafer et al., 2004). These findings, together with our own findings, support the view that GSLs in both axons and myelin may be required for proper localization of Caspr in lipid rafts. However, it is difficult to perform biochemical analysis of axonal adhesion molecules in lipid rafts, since Purkinje neurons are scarce in cerebellar cortex. Furthermore, the excessive partial myelination (with cytoplasmic loop-like structure) in the KO mice suggests that axonal GSLs may play an important role in providing signals required for proper myelination by oligodendrocytes.

Some axons in the mutant mice were surrounded by two concentric myelin sheaths. How do these unusual structures form? In principle there are two possibilities: (1) The additional myelin sheath might invade beneath a preexisting sheath, between the inner loop and the axon surface at the node of Ranvier; or (2) the additional myelin sheath might envelop an entire axon-myelin unit without disrupting existing axon-oligodendrocyte interactions. We cannot definitively distinguish these two possibilities by examining static images. However, we strongly favor the latter mechanism, because at the time of the *Ugcg* gene deletion was induced (at three weeks of age), Purkinje cell axons are already ensheathed by compact myelin

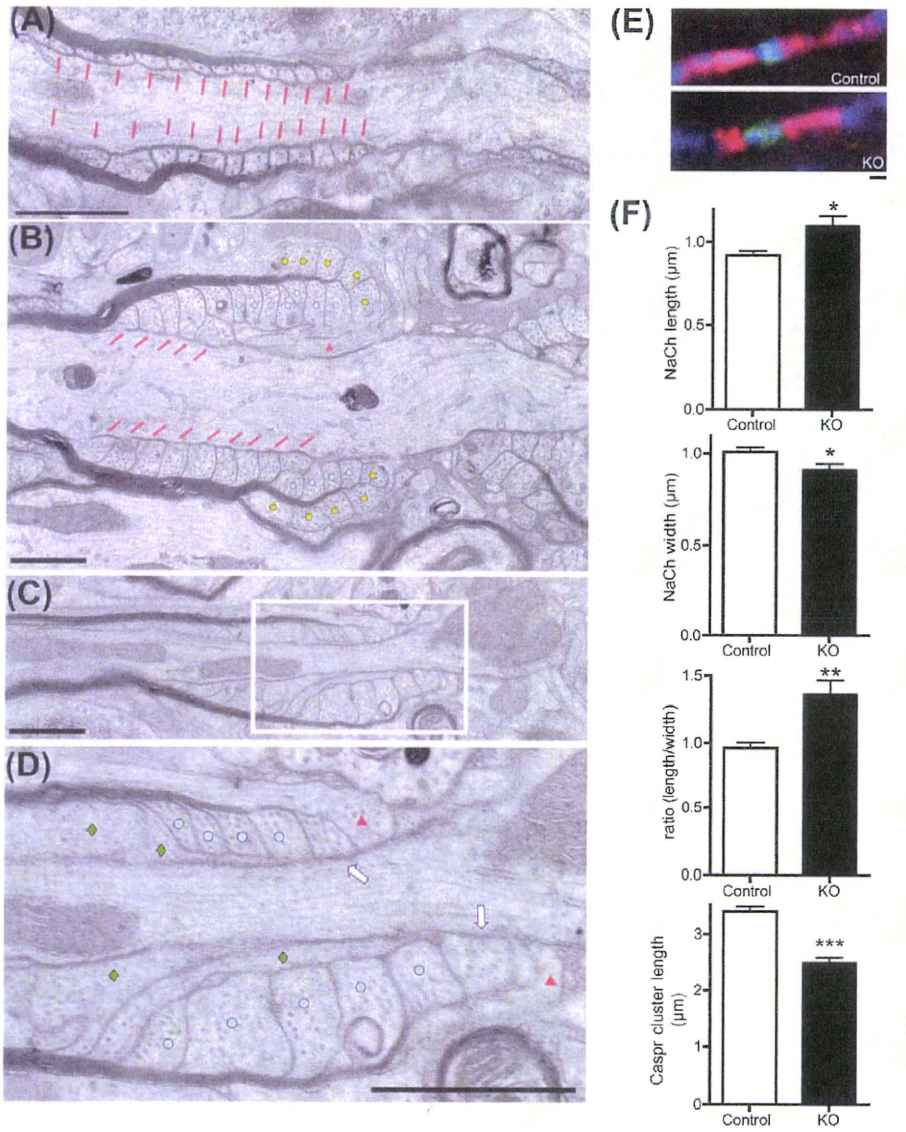

Fig. 7. L7UgcgKO mice exhibit ultrastructural abnormalities at paranodes. Longitudinal section through the paranodal portion of an axon from a control mouse (**A**) and KO mice (**B–D**). A: Normal ultrastructure of node and paranode of a control mouse. The cytoplasmic loops at the paranode are arranged orderly and are attached to the axolemma with a transverse band (TB, red arrow), indicating that at the paranode, the axon is enveloped by oligodendrocyte loops with a continuous TB. B: Abnormal paranode from a 22-week-old L7UgcgKO mouse. A compact myelin sheath consisting of 18 lamellae enwraps this axon. Of the 18 lamellae, nine of the lower and five of the upper paranodal cytoplasmic loops attach themselves onto the axolemma with TB (red arrows). The remaining loops, however, show abnormal contact with the axolemma (circles). The number of lower paranodal cytoplasmic loops contacting the axolemma with a TB is greater than that of the upper loops: nine vs. five normal loops, respectively. This indicates that TBs distribute discontinuously. Some loops (yellow circles) face away from the axon, presumably due to cytoplasmic loop abnormalities. A glial process (red triangle), presumably from an astrocyte, invades the space between the paranodal loops of the oligodendrocyte and axolemma. C: Abnormal paranode from a 14-week-old KO mouse. D: High-magnification image of the white rectangular area in (C). Two paranodal loops (white arrows) directly contact the axolemma. Other paranodal loops (blue circles), however, do not directly contact the axolemma. Deformed loops (green diamonds) attach to the axolemma without TBs. These structures indicate abnormal arrangement of paranodal cytoplasmic loops. These results were observed in all mice of each genotype ($n = 3$). Red triangles indicate processes that are presumably from an astrocyte. **E**: Cerebellar sections were co-immunostained with anti-IP3R1 (blue), anti-Caspr (red), and anti-pan sodium channel (green) antibodies. Elongated sodium channel clusters and shorter Caspr clusters were observed in L7UgcgKO mice. **F**: Quantitation of sodium channel cluster length, width, length-to-width ratio, and Caspr cluster length in lobule V of mid-sagittal sections of 17- to 22-week-old control and L7UgcgKO mice ($n = 3$). $^{*}P < 0.05$; $^{**}P < 0.01$; $^{***}P < 0.001$ compared with control mice. Scale bar: 1 μm (A–E).

(Bouslama-Oueghlani et al., 2003). In addition, it seems inherently unlikely that the adhesion between an axon and myelin membrane, as well as the adhesion between adjacent myelin sheets, could easily be disrupted.

Our results strongly suggest that axonal GSLs are required for axon-myelin interactions at various developmental stages. The binding partner of axonal GSLs in oligodendrocytes is MAG (Yang et al., 1996). MAG is a